IMMUNOLOGY

Generation of an inflammatory niche in a hydrogel depot through recruitment of key immune cells improves efficacy of mRNA vaccines

Emily L. Meany[1], John H. Klich[1], Carolyn K. Jons[2], Tianyang Mao[3], Namit Chaudhary[3,4], Ashley Utz[5,6,7], Julie Baillet[2], Ye E. Song[2], Olivia M. Saouaf[2], Ben S. Ou[1], Shoshana C. Williams[5,8], Noah Eckman[9], Darrell J. Irvine[3,10,11,12,13,4], Eric Appel[1,2,5,14,15]*

Messenger RNA (mRNA) delivered in lipid nanoparticles (LNPs) rose to the forefront of vaccine candidates during the COVID-19 pandemic due to scalability, adaptability, and potency. Yet, there remain critical areas for improvements of these vaccines in durability and breadth of humoral responses. In this work, we explore a modular strategy to target mRNA/LNPs to antigen-presenting cells with an injectable polymer-nanoparticle (PNP) hydrogel technology, which recruits key immune cells and forms an immunological niche in vivo. We characterize this niche on a single-cell level and find it is highly tunable through incorporation of adjuvants like MPLAs and 3M-052. Delivering commercially available severe acute respiratory syndrome coronavirus 2 mRNA vaccines in PNP hydrogels improves the durability and quality of germinal center reactions, and the magnitude, breadth, and durability of humoral responses. The tunable immune niche formed within PNP hydrogels effectively skews immune responses based on encapsulated adjuvants, creating opportunities to precisely modulate mRNA/LNP vaccines for various indications from infectious diseases to cancers.

INTRODUCTION

Over the past three decades, mRNA technology has grown as a therapeutic modality for treatment and prevention of various diseases. It has been developed for protein replacement as well as vaccination against infectious diseases and cancers (*1*–*3*). During the COVID-19 pandemic, mRNA delivered in lipid nanoparticles (LNPs) rose to the forefront of vaccine candidates due to its safety profile, rapid and affordable scalability, and adaptability to emergent variants of concern. Moderna and Pfizer-BioNTech mRNA vaccines proved highly potent and were instrumental in curbing the spread of severe acute respiratory syndrome coronavirus 2 (SARS-CoV-2). Yet, there remain critical areas for improvement of mRNA vaccines, including stability for simpler storage, transport, and deployment in under-resourced parts of the world, as well as enhanced durability and breadth of humoral immune responses (*4*–*6*). In this work, we develop an approach to enhancing mRNA vaccines by targeting of the mRNA/LNPs to antigen-presenting cells (APCs), adjuvanting with molecular adjuvants, and prolonging antigen availability.

[1]Department of Bioengineering, Stanford University, Stanford, CA 94305, USA. [2]Department of Material Science and Engineering, Stanford University, Stanford, CA 94305, USA. [3]Koch Institute for Integrative Cancer Research, Massachusetts Institute of Technology, Cambridge, MA 02139, USA. [4]Howard Hughes Medical Institute, Chevy Chase, MD 20815, USA. [5]Sarafan ChEM- H, Stanford University, Stanford, CA 94305, USA. [6]Stanford Medical Scientist Training Program, Stanford University School of Medicine, Stanford, CA 94305, USA. [7]Stanford Biophysics Program, Stanford University School of Medicine, Stanford, CA 94305, USA. [8]Department of Chemistry, Stanford University, Stanford, CA 94305, USA. [9]Department of Chemical Engineering, Stanford University, Stanford, CA 94305, USA. [10]Consortium for HIV/AIDS Vaccine Development (CHAVD), Scripps Research Institute, La Jolla, CA 92037, USA. [11]Ragon Institute of Massachusetts General Hospital, Massachusetts Institute of Technology and Harvard University, Cambridge, MA 02139, USA. [12]Department of Biological Engineering, Massachusetts Institute of Technology, Cambridge, MA 02139, USA. [13]Department of Materials Science and Engineering, Massachusetts Institute of Technology, Cambridge, MA 02139, USA. [14]Wood Institute for the Environment, Stanford University, Stanford, CA 94305, USA. [15]Department of Pediatrics (Endocrinology), Stanford University, Stanford, CA 94305, USA.
*Corresponding author. Email: eappel@stanford.edu

APCs are key immune cells responsible for processing and presenting antigen to train the adaptive arm of the immune system—T and B cells—and a desirable target for mRNA/LNP transfection (*7*). A recent study by Hassett *et al.* (*8*) at Moderna found macrophages and dendritic cells (DCs) infiltrating the site of administration, as well as off-target adipocytes, fibroblasts, and epithelial cells in these tissues, took up mRNA and expressed protein following intramuscular injection in nonhuman primates (NHPs), with peak expression 24 hours postinjection. While antigen produced by non-APCs could contribute to a meaningful immune response, improving antigen production and delivery to professional APCs is expected to be beneficial for priming both B and T cell responses. Many groups have worked to improve APC targeting by modifying LNPs with targeting moieties like antibodies or mannose, as well as altering lipid chemistries to bias their biodistribution (*9*–*12*). While many of these strategies have demonstrated improved cell-type targeting, they often involve cumbersome large-scale screening campaigns and complex lipid chemistries that can alter LNP bioactivity since the lipids are known to contribute to transfection efficiency and adjuvanting effects of LNPs (*13*, *14*). Moreover, each newly designed lipid will be regulated as a novel chemical entity, thereby limiting translatability. mRNA/LNP vaccines could benefit from a more modular method to target APCs and limit off-target cell transfection without alterations to the existing LNP chemistries.

For the past decade, there has been a growing body of literature exploring how biomaterials like hydrogels, polymer microparticles, or mesoporous silica rods can interface with the immune system (*15*–*22*). Several groups have explored biomaterials to recruit circulating immune cells for a variety of applications, from sequestration to prevent autoimmune disease onset, to forming proxy-metastatic sites for biopsy-based disease tracking, and even for in vivo restimulation of CAR-T cells (*15*–*17*). Others have applied microparticle platforms to interface with DCs to formulate a tolerogenic vaccine (*21*). While these materials vary widely in composition and application, the

concept of attracting immune cells to a de novo niche in vivo could be a means to target unmodified mRNA/LNPs and vaccine cargo to key APCs.

In addition to better APC targeting, adjuvanting mRNA/LNP vaccines could improve the overall magnitude and quality of the vaccine response. Adjuvants are immunostimulants that can drive potent immune responses, as well as tailor a response toward T helper 1 (T_H1), T_H2, or other phenotypes important in mounting successful responses against different diseases. Yet, the impact of adjuvants on mRNA vaccines remains poorly characterized, with evidence of both benefits and detriments previously reported (*23*–*25*). Excessive stimulation of innate cells can hamper mRNA expression and negatively affect vaccine efficacy. Seemingly contrary to this, some groups have found incorporation of pathogen-associated molecular pattern adjuvants like Toll-like receptor agonists (TLRas) can improve mRNA vaccine efficacy, particularly TLR2/6a, 7/8a, and 9a (*26*–*29*). While promising, these studies required lipid modification, reformulation, or even use of a different delivery modality entirely, and are not readily applicable within existing mRNA/LNP vaccines. Furthermore, the need to modify LNPs to incorporate adjuvants severely limits which adjuvants can be used and compromises the ability to directly compare impacts of adjuvants across platforms. An off-the-shelf technique allowing modular selection of single or combination adjuvants will be especially beneficial to cater to different disease needs as mRNA vaccines expand in use to other infectious diseases, anticancer vaccines, and even tolerogenic vaccines (*30*).

Last, it has been shown that extended delivery of antigen can improve germinal center reactions and overall vaccine responses to subunit vaccines (*31*–*33*). However, sustained delivery is difficult to achieve with mRNA vaccines as mRNA translation is transient, and mRNA is prone to hydrolysis and degradation following injection, even with advances in base modifications and LNP delivery vehicles. Previous efforts have pursued prolonged antigen availability through increased expression with self-amplifying RNA (saRNA), but LNPs for saRNA can be difficult to formulate because of the larger mRNA required to encode the target antigen as well as the replication machinery (*34*). A means to extend the expression and availability of antigen with standard mRNA vaccines could further improve their efficacy.

In this work, we explored a modular strategy to adjuvant mRNA/LNPs and target their uptake by APCs via encapsulation in an injectable, dynamic hydrogel depot technology known to attract and activate key immune cells in vivo to form a local immunologic niche. We leveraged polymer-nanoparticle (PNP) hydrogels formed through dynamic, noncovalent interactions between hydrophobically modified hydroxypropylmethylcellulose (HPMC-C_{12}) and poly(ethylene glycol)-block-poly(lactic acid) nanoparticles (PEG-PLA NPs) (*35*). It may be useful to note that "NP" in PNP refers to PEG-PLA polymer nanoparticles, which form a structural motif in the hydrogel, while NP in LNP refers to lipid nanoparticles that encase mRNA for protection and cellular delivery. These PNP hydrogels are biocompatible and inert, yet they attract immune cells and form an immune niche in vivo when loaded with inflammatory cargo like vaccines and adjuvants (*36*–*38*). While these hydrogels have a small effective mesh size capable of entrapping diverse molecular cargo, their dynamic cross-links allow cells to exert forces and actively migrate into the material and interact with loaded cargos (*39*–*45*). We hypothesized that these materials would promote targeting of mRNA/LNPs to infiltrating APCs, as well as allow for admixing of different adjuvants for a modular, off-the-shelf platform to study and compare adjuvanting of mRNA vaccines. The ability to admix different adjuvants allows for tuning of the inflammatory microenvironment where APCs encounter the mRNA/LNPs across a spectrum of inflammatory states, from highly inflammatory for anticancer applications to tolerogenic for applications like diabetic "inverse" vaccines. We also hypothesized that sequestering mRNA/LNPs within the hydrogel would slow the diffusion and penetration of ribonucleases (RNases) and other enzymes, allowing for extended delivery and translation of mRNA, improving the immune response.

We first demonstrated the plasticity of the PNP hydrogel immunologic niche in vivo in response to mRNA/LNPs alone or with two separate TLRas, synthetic monophosphoryl lipid A (synthetic MPLA, denoted MPLAs; TLR4a), or 3M-052 (TLR7/8a). Flow cytometry analyses revealed clear skewing of the cellular milieu based on encapsulated cargo, with transient infiltration of different immune cells such as neutrophils, monocytes, or natural killer (NK) cells influenced by different cargos. Using a model mRNA cargo, we examined the mRNA translation in this in vivo niche and found key APCs actively take up LNPs and produce the encoded protein. We investigated the impact of distinct PNP hydrogel–based immune niches on the humoral and cellular responses to a commercially available SARS-CoV-2 mRNA vaccine compared with a clinical control bolus administration. Both PNP hydrogels alone and with coencapsulated adjuvants improved the magnitude, durability, and breadth of humoral immune responses, the functionality of the antibodies produced, and the systemic T cell response. We further investigated the lymph node (LN) germinal center reactions underlying these improvements in vaccine response and found that PNP hydrogels, particularly when adjuvanted, increased the magnitude and quality of the germinal center reaction to mRNA/LNP vaccines.

RESULTS

Characterization and in vitro validation of supramolecular hydrogels loaded with mRNA/LNPs

In this work, we leveraged the unique mechanical properties and modularity of PNP hydrogels to form an immune niche and selectively deliver mRNA/LNPs to recruited APCs. Following subcutaneous injection in mice, migratory immune cells are recruited to the injected hydrogel depot, where they can exert forces and infiltrate the dynamically cross-linked material (Fig. 1A). Once cells enter the PNP hydrogel depot, they encounter the mRNA/LNPs and can be transfected before migrating to the draining LN to initiate germinal center reactions. We hypothesized that we could skew the cell populations in the hydrogel immune niche by incorporating different inflammatory cargo such as potent TLR4a (MPLAs) or TLR7/8a (3M-052) adjuvants. These adjuvants have shown promise in other vaccine formulations, as well as clinical vaccines (e.g., the human papillomavirus vaccine by GSK is adjuvanted with ASO4 comprising MPL/alum) (*46*–*48*). In addition, both adjuvants have lipid moieties that promote retention in the PNP hydrogel (*45*).

PNP hydrogels are formed through simple mixing of HPMC-C_{12} and PEG-PLA NPs. These components interact in a multivalent, noncovalent fashion to form an injectable, shear-thinning, and self-healing dynamic hydrogel. Multiple cargos can be admixed into the hydrogel, including commercially available mRNA vaccines, other mRNA/LNPs, and adjuvants (Fig. 1, B and C). We first sought to characterize how commercially available SARS-CoV-2 mRNA vaccine

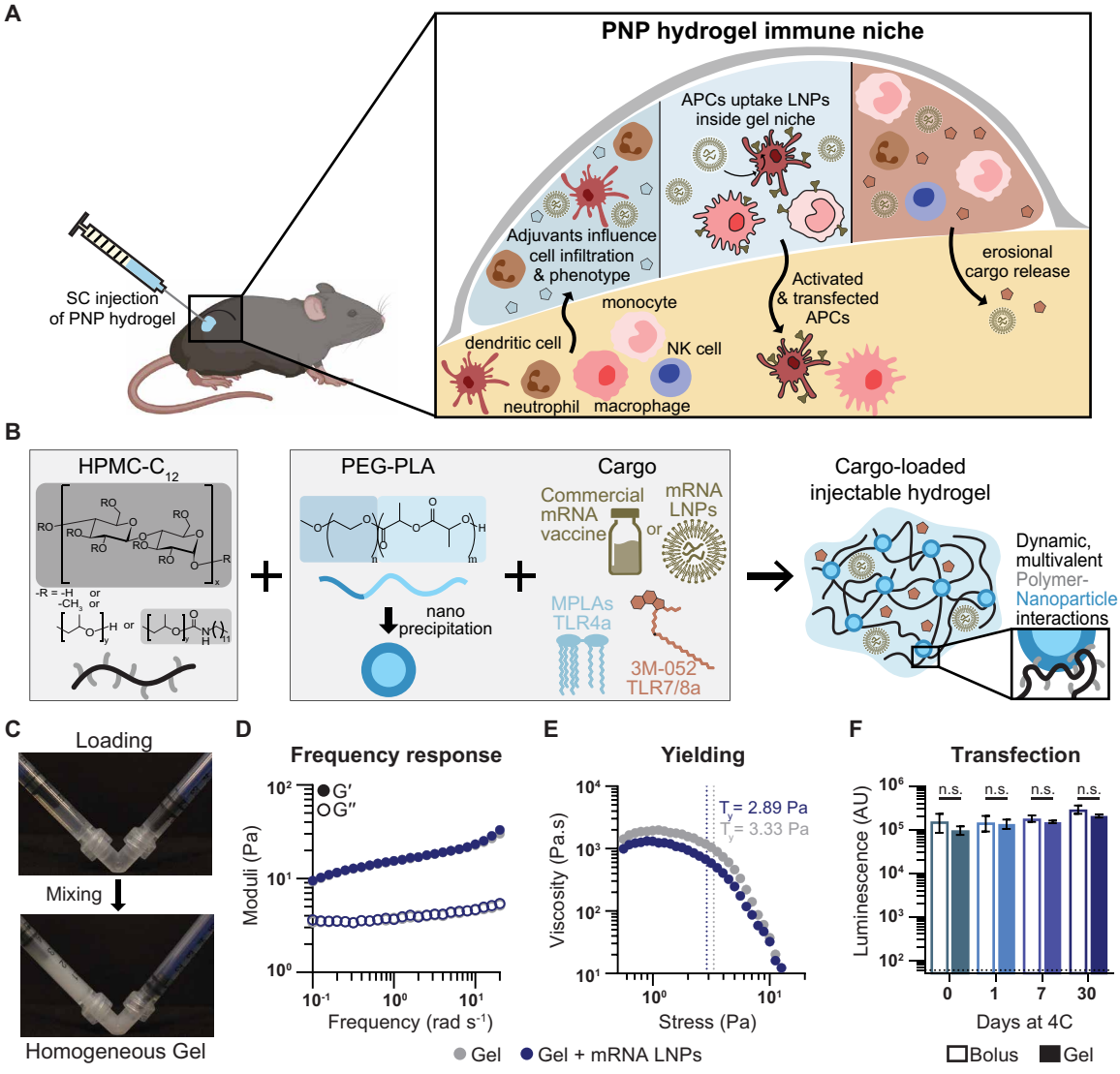

Fig. 1. Schematic of immune niche in PNP hydrogels comprising mRNA/LNPs. (**A**) PNP hydrogels injected subcutaneously allow immune cell infiltration and interaction with loaded cargo. Incorporation of various adjuvants influences the immune niche. Cells within the niche take up mRNA/LNPs, express the delivered protein, and migrate to initiate immune responses in the draining LNs. (**B**) PNP hydrogels comprise HPMC-C_{12} and PEG-PLA NPs. Cargo, including mRNA/LNP vaccines and molecular adjuvants, can be easily mixed with the polymer components to form a dynamic hydrogel. (**C**) Hydrogel components are loaded into two syringes, attached with an elbow, and mixed to form a homogenous material, preloaded in a syringe and ready for administration. (**D**) Frequency shear rheology shows that PNP-0.5-5 material is solid-like across timescales, and mRNA/LNPs (50 μg ml^{-1}) do not alter this. (**E**) Stress-ramp data show static yield stress, defined as the intersection of tangent lines for the plateau and yielding regimes, for PNP-0.5-5 hydrogel is not affected by LNPs. (**F**) Luminescent signal from RAW-Blue macrophages dosed with luciferase mRNA/LNPs in either PBS bolus or PNP hydrogel after storage in that condition for up to 30 days at 4°C. Hydrogels do not affect transfection or stability of mRNA/LNPs. Data shown as means ± SD, $n = 3$ to 4, and statistics are multiple unpaired two-tailed *t* tests run in GraphPad Prism with false discovery rate correction using two-stage step-up method of Benjamini, Krieger, and Yekutieli.

affects key mechanical properties of the PNP hydrogels. Frequency sweep oscillatory shear rheology showed that the selected formulation, PNP-0.5-5 (0.5 wt % HPMC-C_{12}; 5 wt % NPs), was solid-like over tested frequencies and was not affected by mRNA/LNP incorporation (Fig. 1D). Further, stress ramp experiments showed clear pre-yielded and yielded regimes with a yield stress of approximately 3 Pa (Fig. 1E). These results indicated that these materials would form disk-like depots in the subcutaneous space (*49*). High-to-low shear-ramp and step-shear experiments showed that PNP-0.5-5 hydrogels were shear thinning and capable of repeatedly returning to a high viscosity state following high-shear events, indicating that the hydrogel could be injected through standard needles and recover as a solid-like depot following injection (fig. S1).

Having shown that mRNA/LNPs did not disrupt hydrogel material properties, we next confirmed that mRNA/LNPs were unaffected by loading within PNP hydrogels. We assessed mRNA/LNP transfection efficiency in vitro with luciferase-encoding mRNA/LNPs mimicking the lipid formulation used in Moderna's Spikevax vaccine. In these assays, we diluted the luciferase mRNA/LNPs into phosphate-buffered saline (PBS) or incorporated them into PNP-0.5-5 hydrogels

and stored at 4°C for 0, 1, 7, and 30 days before delivering to RAW-Blue macrophages and measuring transfection efficiency via bioluminescence after 24 hours (Fig. 1F). We selected this cell line to be representative of the phagocytic cells and APCs we hypothesized targeting with the hydrogel niche and because macrophages were among the most abundant cell types found to infiltrate PNP-2-10 hydrogels in previous work (*36*). Visual inspection of plate wells at 24 hours showed that the hydrogel material was mostly dissolved and did not form a coherent "depot." Unlike subcutaneous injection where PNP hydrogels form a persistent depot with cargo release determined primarily by erosion, this in vitro assay involved a small volume of hydrogel injected into an excess of liquid media, which likely led to rapid dissolution and release of most mRNA/LNP cargo. Transfection efficiency remained unchanged for mRNA/LNPs formulated into PNP hydrogels compared with delivery in bolus at all tested storage times. These stability data agreed with the product stability for Moderna Spikevax (4°C for 30 days) and demonstrated that PNP hydrogel–based formulations did not impede transfection capacity of loaded mRNA/LNPs.

Tunable immune niche formed within PNP hydrogel in vivo

One unique feature of PNP hydrogels is that their nanoscale mesh size allows retention of small cargos, yet their dynamic cross-links allow immune cells to migrate into the material in response to inflammatory cargo (*50*). We used flow cytometry to phenotype the immune niche within the PNP hydrogel depot over time in response to mRNA/LNPs with and without MPLAs or 3M-052 adjuvants. We injected C57BL/6 mice subcutaneously on the flank with 100 μl of PNP hydrogel containing 1 μg of mCherry mRNA/LNPs, either alone or with adjuvants, and excised the hydrogel depots at days 3 and 7 for single-cell flow cytometry (Fig. 2A and figs. S2 and S3). PNP-0.5-5 hydrogels clearly formed persistent depots that were easy to excise and, upon visual inspection out to 3 weeks, did not have evidence of gross fibrosis or capsule formation around the material (Fig. 2B and fig. S4). Prior work has also shown that stiffer PNP hydrogels (PNP-2-10) fully erode within 8 weeks following injection without visible gross capsule or fibrosis remnants (*36*). The hydrogels contained more than a million $CD45^+$ leukocytes on day 3 (1.35×10^6) and significantly more in adjuvant-loaded hydrogels (2.23×10^6 with MPLAs, $P = 0.025$, and 2.27×10^6 with 3M-052, $P = 0.033$ compared to LNP-only hydrogels). PNP hydrogels with mRNA/LNPs hosted almost double the cells found in empty PNP hydrogels (0.78×10^6), likely due to the inherent immunogenicity of mRNA/LNPs, and PNP hydrogels loaded with Moderna Spikevax showed comparable infiltration to ones loaded with mCherry mRNA/LNPs (fig. S5). Over time, cells migrated out of PNP hydrogels and the depot dissolved away. On day 7, we found fewer, but still a measurable number of, cells in LNP-only hydrogels (0.20×10^6), while adjuvanted hydrogels maintained more cells (0.34×10^6 with MPLAs and 0.65×10^6 with 3M-052) (Fig. 2C). The hydrogel depots measured approximately 100 mm^3 on day 2 and 70 to 75 mm^3 on day 7, indicating a cell density of 3 to 23×10^6 ml^{-1}. For reference, the average cell density in LNs across animals studied for germinal center responses later in this work was ~110×10^6 ml^{-1} (*51*). Impressively, the PNP hydrogel depots sustained cell densities up to a quarter of that of LNs undergoing active vaccine responses.

We then sought to examine the plasticity of the PNP cell niche across time and with the different adjuvant cargos using Uniform Manifold Approximation and Projection (UMAP) (Fig. 2D). Overlaying the generated UMAP with gated cell populations, we found that cell types fell within clear UMAP clusters and observed distinct and dramatic differences among groups and time points. We quantified these differences with each cell type's percentage of total $CD45^+$ leukocytes, as well as absolute count per gel (Fig. 2E and fig. S6). On day 3, there were clear differences across groups in neutrophil, DC, and monocyte populations. Neutrophils composed 59 and 42% of $CD45^+$ cells in the MPLAs and 3M-052 groups but only 24% in LNP-only hydrogels. Adjuvanted hydrogels also had more monocytes compared to LNP-only hydrogels, significantly so for 3M-052 hydrogels ($P = 0.021$). Unexpectedly, significantly fewer DCs were observed in 3M-052 hydrogels compared to LNP-only and to MPLAs hydrogels ($P = 0.0004/0.0007$, respectively). By day 7, most cell types across all hydrogel groups had decreased, excepting an influx of NK cells into 3M-052 hydrogels, which then constituted 28% of $CD45^+$ cells. Adjuvanted hydrogels also retained substantially more neutrophils and monocytes at day 7 compared to LNP-only hydrogels ($P = 0.0010/0.006$ and $P < 0.0001/0.0024$ for each cell type, respectively, in 3M-052/MPLAs hydrogels).

We further visualized different subpopulations and phenotypes of macrophages and DCs with UMAP and found monocyte-derived macrophages ($Ly6C^{hi}$) and DCs (mDCs) clearly clustered nearer to monocytes (Fig. 2, F and G). Macrophage counts in all PNP hydrogel groups were similar on days 3 and 7, but the percentage they composed of $CD45^+$ cells, and their phenotypes, were distinct. On day 3, macrophages made up 8 to 19% of $CD45^+$ cells in all hydrogels and mostly spanned the UMAP spectrum, except for in 3M-052 hydrogels where they were primarily $Ly6C^{hi}$. By day 7, macrophages made up 24% of $CD45^+$ cells in MPLAs and 51% in LNP-only hydrogels and had shifted in phenotype to be almost entirely $Ly6C^{lo}$. In contrast, they accounted for 12% of $CD45^+$ cells in 3M-052 hydrogels and fell almost entirely within the monocyte-derived region of the UMAP. We also observed a slight increase in DCs in MPLAs hydrogels from days 3 to 7, with a larger population specifically of inflammatory mDCs compared to LNP-only hydrogels.

Overall, these data clearly indicate that immune cells migrate to injected PNP hydrogel depots and form highly plastic and tunable inflammatory niches in response to different adjuvant cargos. The ability of PNP hydrogels to retain vaccine cargo while enabling cellular infiltration is one that we can leverage to target mRNA/LNPs to key APCs under specific conditions, such as being surrounded by unique cellular milieu whose inflammatory state can be skewed with different cargos.

Expression pattern of delivered mRNA in PNP hydrogel cell niche

Following the characterization of the highly plastic cell niche within the PNP hydrogel depot, we wanted to understand whether cells within the niche took up LNPs and translated the delivered mCherry mRNA (Fig. 3A). We found that cells isolated from hydrogels on days 3 and 7 were $mCherry^+$ by flow cytometry with mean fluorescent intensity greater than background signal from PNP hydrogels containing non-mCherry mRNA/LNPs (Fig. 3B and fig. S7). We quantified the count and proportion of $CD45^+$ $mCherry^+$ cells and observed 3.8, 2.2, and 6.9 ($\times 10^3$) cells expressed mCherry on day 3 in LNP-only, MPLAs, and 3M-052 hydrogels, respectively, making up 0.3, 0.1, and 0.3% of all $CD45^+$ cells (Fig. 3, C and D). Cells within PNP hydrogels maintained mCherry expression from delivered mRNA/LNPs through day 7, with double the number of cells found expressing mCherry in 3M-052 hydrogels (12.3×10^3, or 2.1% of all

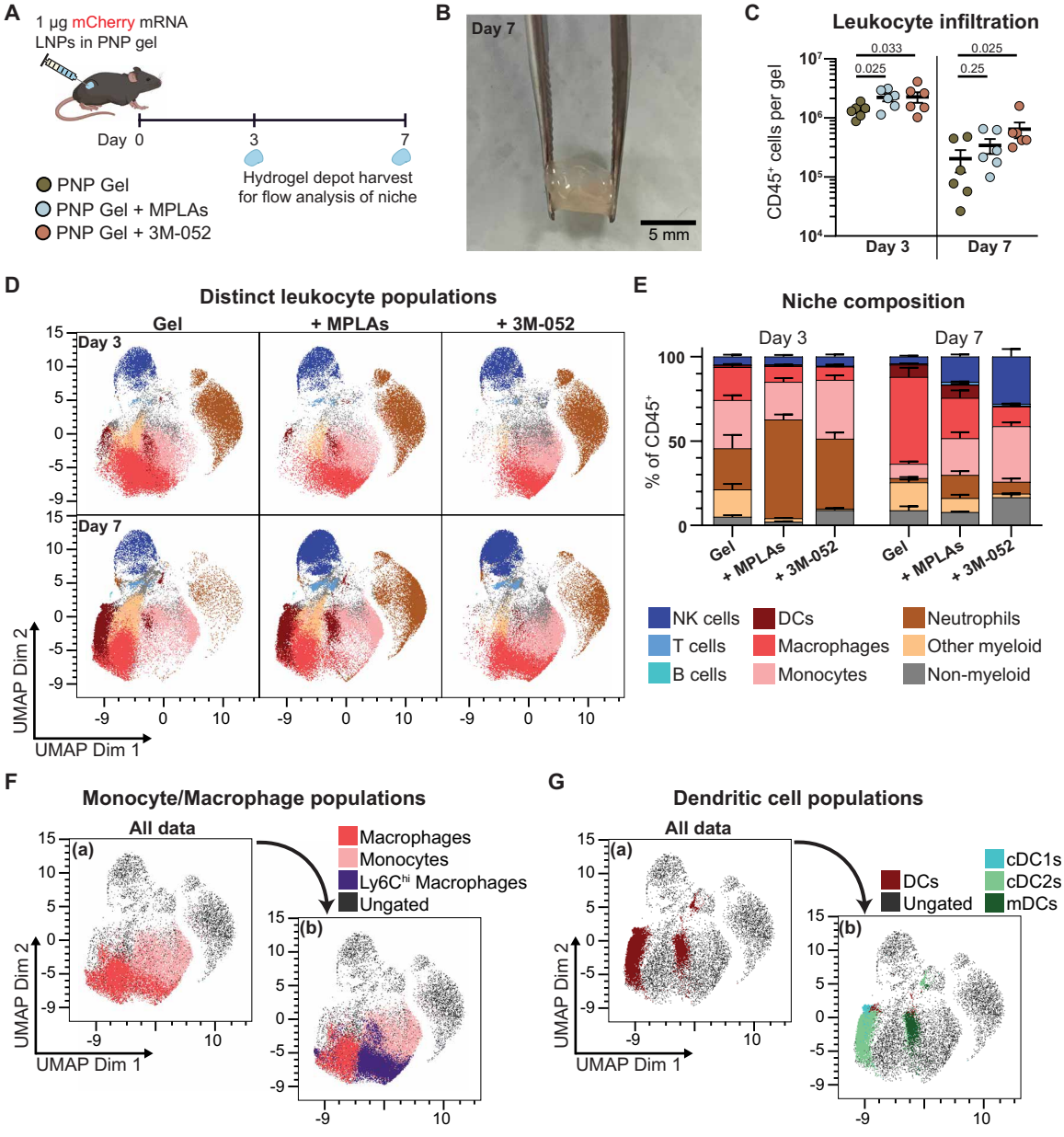

Fig. 2. Characterization of in vivo immune niche in PNP hydrogels. (**A**) PNP hydrogels loaded with mCherry mRNA/LNPs injected subcutaneously were excised at days 3 and 7 for dissociation and analysis of cells with flow cytometry. (**B**) Excised PNP hydrogel depot on day 7 showing size and no visible evidence of gross fibrosis. (**C**) Counts of CD45$^+$ leukocytes per gel show robust infiltration on both days, with increased infiltration with adjuvant cargo. Data shown as means ± SEM, $n = 6$. Statistical values shown are P values <0.25 obtained from general linear model (GLM) fitting and Tukey post hoc multiple comparison test in JMP. (**D**) Changes in cell type populations visualized with UMAPs. (**E**) Quantification of cell types in each hydrogel niche as percentages of all gated CD45$^+$ cells. Data shown as means + SEM, $n = 6$. (**F**) UMAP visualization showing relation of Ly6C^{hi} macrophage subpopulation to macrophages and monocytes. (**G**) UMAP visualization of DC subpopulations highlighting differences between classical DCs (cDC1s and 2 s) and mDCs.

CD45$^+$ cells), suggesting that additional cells began mRNA translation after 72 hours. This was particularly promising as a recent study by Hassett *et al.* (*8*) at Moderna demonstrated that mRNA levels in NHPs were depleted at the injection site by 72 hours with peak protein expression at 24 hours, yet we saw increasing protein expression in 3M-052 hydrogels as late as day 7. MPLAs hydrogels also had similar counts of mCherry$^+$ cells from days 3 to 7 (2.2×10^3 and 2.7×10^3), suggesting extended expression and prolonged antigen availability compared to the previously reported peak at 24 hours. A deeper examination of the cell types translating delivered mRNA revealed that the mCherry$^+$ cells were overwhelmingly APCs—DCs, monocytes, and macrophages—across all gel groups (Fig. 3E and fig. S8). Monocytes comprised the majority of mCherry$^+$ cells at 49% and 70% of mCherry$^+$ cells in MPLAs and 3M-052 hydrogels, whereas DCs made up 22 and 1% for each group respectively on day 7.

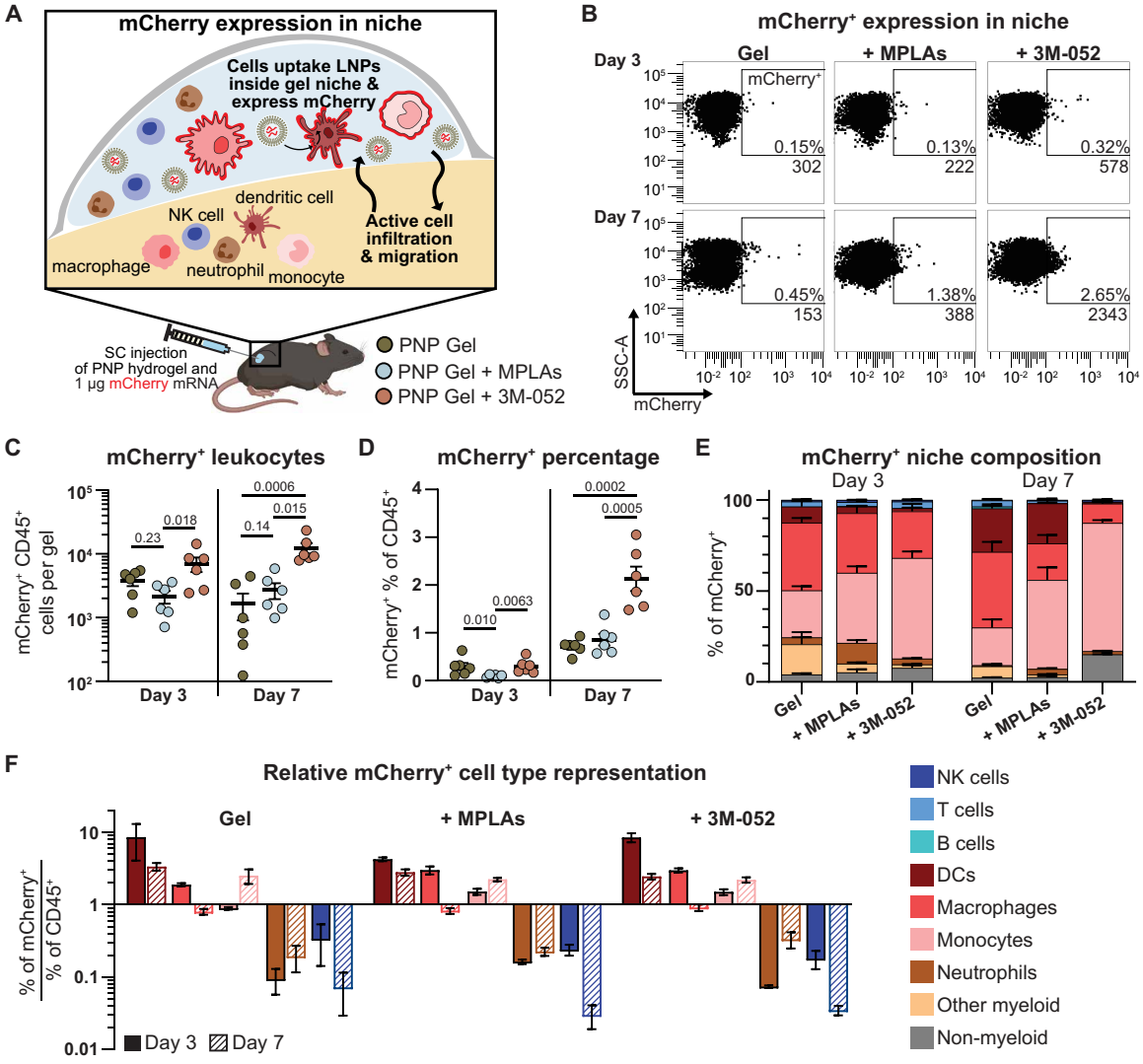

Fig. 3. Characterization of mRNA expression in PNP hydrogel immune niche. (**A**) Immune cells infiltrate injected PNP hydrogels loaded with mCherry mRNA/LNPs in vivo, take up LNPs, and express reporter mCherry protein. These cells can be quantified on days 3 and 7 following hydrogel excision with flow cytometry. (**B**) Representative flow plots showing mCherry signal in CD45$^+$ cells with percentage of CD45$^+$ parent and total cell counts. (**C**) The count of mCherry expressing CD45$^+$ leukocytes per gel and (**D**) those cells as a percentage of all CD45$^+$ cells. Adjuvants increase the absolute number and percentage of CD45$^+$ cells expressing the delivered mRNA. Data shown as means ± SEM, $n = 6$. Statistical values shown are P values <0.25 obtained from GLM fitting and Tukey post hoc multiple comparison test in JMP. (**E**) Quantification of cell types in the mCherry$^+$ subniche per hydrogel as percentages of all gated CD45$^+$ mCherry$^+$ cells. Data shown as means + SEM, $n = 6$. (**F**) Ratio of the proportion each cell type makes up of the mCherry$^+$ subniche to its percentage of the full CD45$^+$ niche. Values of one indicate that a cell is represented equally in the mCherry$^+$ subniche as in the full gel. Values under one indicate that fewer cells are mCherry$^+$ than expected based on that cell type's percentage of the CD45$^+$ niche, and vice versa for values over one (overrepresented in mCherry$^+$ subniche). Data shown as means ± SEM, $n = 6$.

Considering the obvious differences observed in overall CD45$^+$ cell niche compositions, yet relatively similar mCherry$^+$ subniche compositions across groups (primarily APCs), we sought to examine whether certain cell types were specifically enriched in the mCherry$^+$ subniche. To do this, we took the ratio of each cell type percentage of mCherry$^+$ cells divided by the same cell type's percentage of all CD45$^+$ cells (Fig. 3F). In this way, cell types that make up the same percentage of mCherry$^+$ cells as they do all CD45$^+$ cells would have a ratio of one. Similarly, ratios less than one would indicate that fewer of that cell type are mCherry$^+$ than expected given their frequency in the overall CD45$^+$ niche, and vice versa for values over one where cell types are enriched for mRNA translation. From this, we observed that APCs were overrepresented in the mCherry$^+$ subniche, while neutrophils and NK cells, despite encompassing a large fraction of the overall CD45$^+$ cell niche, were underrepresented in the mCherry$^+$ subniche. Looking at the fraction of each cell type that was expressing mCherry, less than 0.08% of NK cells and 0.8% of neutrophils expressed mCherry across all groups while up to 1.9, 4.6, and 5.3% of macrophages, monocytes, and DCs, respectively, expressed mCherry on day 7 (fig. S9). Similar analysis can be found in the supplement for B and T cells, which made up a very small fraction of the overall CD45$^+$ cell niche, and for other and nonmyeloid cells (fig. S10). These observations indicated that mRNA/LNPs incorporated into PNP hydrogels successfully transfected APCs, a key cell type for

training adaptive immune responses. Further, the transfected cell types did not change substantially with different adjuvant cargo, whereas the surrounding cell niche did, providing a means to independently tune the context in which APCs express and present antigen. This approach presents a key opportunity when considering mounting different types of immune responses, such as anticancer or tolerogenic, where the context of antigen processing and presentation is critical.

Improved humoral and cellular response to commercial mRNA vaccine with PNP hydrogels

We next wanted to evaluate the impact of PNP hydrogels with and without adjuvants (and their corresponding cell niches) on the response to an mRNA/LNP vaccine. The modularity of PNP hydrogels allows simple incorporation of commercially available vaccines, like Moderna's Spikevax vaccine encoding the full spike protein of SARS-CoV-2, in a simple off-the-shelf manner with and without adjuvants. We first evaluated two material formulations, PNP-0.5-5 and PNP-1-5, to assess any effects of material mechanical properties on the humoral response (fig. S11). PNP-1-5 hydrogels were an order of magnitude stiffer than PNP-0.5-5 hydrogels, resulting in a more persistent depot with slower release kinetics and potentially limited cellular infiltration at early time points. As mRNA degrades rapidly by hydrolysis, we hypothesized earlier cellular infiltration into the softer material could be beneficial. Further, the PNP-1-5 material showed reduced transfection in vitro compared with bolus and PNP-0.5-5, suggesting challenges with maintaining mRNA/LNP stability in higher HPMC-C_{12} polymer content material, which would require additional optimization (fig. S11B). We therefore moved forward with the previously characterized PNP-0.5-5 formulation.

We delivered 0.25 μg of mRNA/LNPs (Moderna Spikevax bivalent vaccine encoding WH1 and BA.4/.5) in a 100-μl subcutaneous injection in either PBS, the current clinical standard, or PNP-0.5-5 hydrogel with or without MPLAs or 3M-052. We determined group sizes using Mead's resource equation to optimize study power by targeting 10 to 20 error degrees of freedom (eDFs) and immunized $n = 5$ to 6 animals per group for a total of 23 to 24 animals and 19 to 20 eDFs (*52*). Sensitivity analysis with G*Power software confirmed that our study design was powered at 0.8 (1-β) and $\alpha = 0.05$ to see large effect sizes of $f = 0.76$, sufficient to identify meaningful improvements or noninferiority to clinical standard bolus (*53*). We dosed mice at weeks 0 (prime) and 8 (homologous boost) and collected serum for antibody titer evaluation over 6 months (Fig. 4A). We immunized a separate cohort of animals and evaluated the T cell response via interferon-γ (IFN-γ) enzyme-linked immunosorbent spot assay (ELISpot) at week 10 (2 weeks post-boost). Serum titer enzyme-linked immunosorbent assays (ELISAs) against WH1 spike protein 8 weeks post-prime showed that five in six animals exhibited measurable titers in the PNP hydrogel group compared to only one in six in the bolus control group (Fig. 4B). Animals immunized with PNP hydrogel vaccines containing 3M-052 produced significantly higher titers compared to bolus ($P = 0.016$), as did those dosed with PNP hydrogel vaccines containing MPLAs, albeit not statistically significant ($P = 0.090$). When additional animals from the ELISpot cohort were evaluated for titers at week 8, these trends became more evident and significant, with PNP hydrogel animals showing higher titers than bolus and adjuvanted hydrogels even higher titers ($P = 0.047/0.0030/0.0005$ for PNP only/MPLAs/3M-052 compared to bolus) (fig. S12). At 4 months post-boost, the average titer of animals in adjuvanted hydrogel groups was higher than that of bolus control animals, and animals that received PNP hydrogel vaccines with 3M-052 exhibited average titers more than fivefold higher than those that received bolus control or LNP-only hydrogel vaccines, although these trends were not statistically significant ($P = 0.26/0.16$, respectively) (Fig. 4C). Titer improvements over bolus were observed most significantly in the pre-boost time frame, with PNP hydrogel alone and with MPLAs consistently producing higher titers over bolus and PNP hydrogel with 3M-052 further increasing titers (Fig. 4D). Total pre-boost antibody exposure, measured by area under the curve (AUC), was higher for PNP hydrogel–immunized animals compared to bolus and significantly so for those immunized with adjuvanted PNP hydrogels ($P = 0.072/0.041/0.0038$ for PNP only/MPLAs/3M-052 compared to bolus). Following out to 4 months, animals with PNP hydrogel and 3M-052 maintained higher, but not significant, overall antibody exposure compared to bolus (Fig. 4E).

To understand the role of adjuvant alone in the improved titers, we immunized mice with bolus mRNA/LNPs with or without 3M-052 on alum as a clinically relevant adjuvant (fig. S13). Titer data out to week 8 and AUC analysis showed that soluble adjuvant provided no significant improvement over bolus, indicating the importance of PNP hydrogels in forming a cellular niche and colocalizing mRNA/LNPs and adjuvant.

Considering that durability is a concern with current commercial mRNA/LNP vaccines, we extracted an average antibody half-life using parametric bootstrapping on titer data following the post-boost peak (week 10 for bolus and week 12 for hydrogel groups, $n = 1000$ runs) (Fig. 4F). The PNP hydrogels increased antibody decay half-life by 11% over the bolus control, and adjuvanted PNP hydrogel groups increased antibody decay half-lives by 143 and 68% (MPLAs and 3M-052, respectively, $P < 0.0001$) over the bolus control. These enhancements represent a shift in half-life from 1 month for bolus delivery to upward of 2.5 months for adjuvanted PNP hydrogels.

We next examined the functionality of the antibody response based on neutralization, as well as the T cell response. Current mRNA/LNP vaccines are relatively successful in these metrics, and we wanted to verify that PNP hydrogels were noninferior to bolus at time points where bolus titers were highest. We performed SARS-CoV-2 BA.4/.5 pseudotyped lentivirus neutralization assays at week 13 post-prime (week 5 post-boost) and found no significant difference in infectivity comparing bolus to PNP hydrogel groups and even a trend toward enhanced neutralization (i.e., lower infectivity) in adjuvanted PNP hydrogel groups (Fig. 4G and fig. S14). Only PNP hydrogel immunized groups yielded infectivities below 10% at 1:50 serum dilution, with two, one, and two of six animals in PNP only, with MPLAs, and with 3M-052 groups, respectively. PNP hydrogels with 3M-052 also exhibited a modestly lower mean infectivity of 29.3% compared to 41.4 to 51.4% for other groups. We next assessed functional T cell responses to WH1 spike peptides via ELISpot for IFN-γ–producing splenocytes, a proxy for IFN-γ–producing T cells, at week 10 post-prime (week 2 post-boost). Vaccine delivery in PNP hydrogels was again comparable to bolus, and adjuvanting with 3M-052 produced a moderately more robust T cell response (Fig. 4H). Together, the humoral and cellular responses to SARS-CoV-2 mRNA/LNP vaccines are improved or not impaired by delivery in PNP hydrogels and especially so with adjuvanted PNP hydrogels, whereas no humoral improvement is achieved with standard bolus adjuvanting.

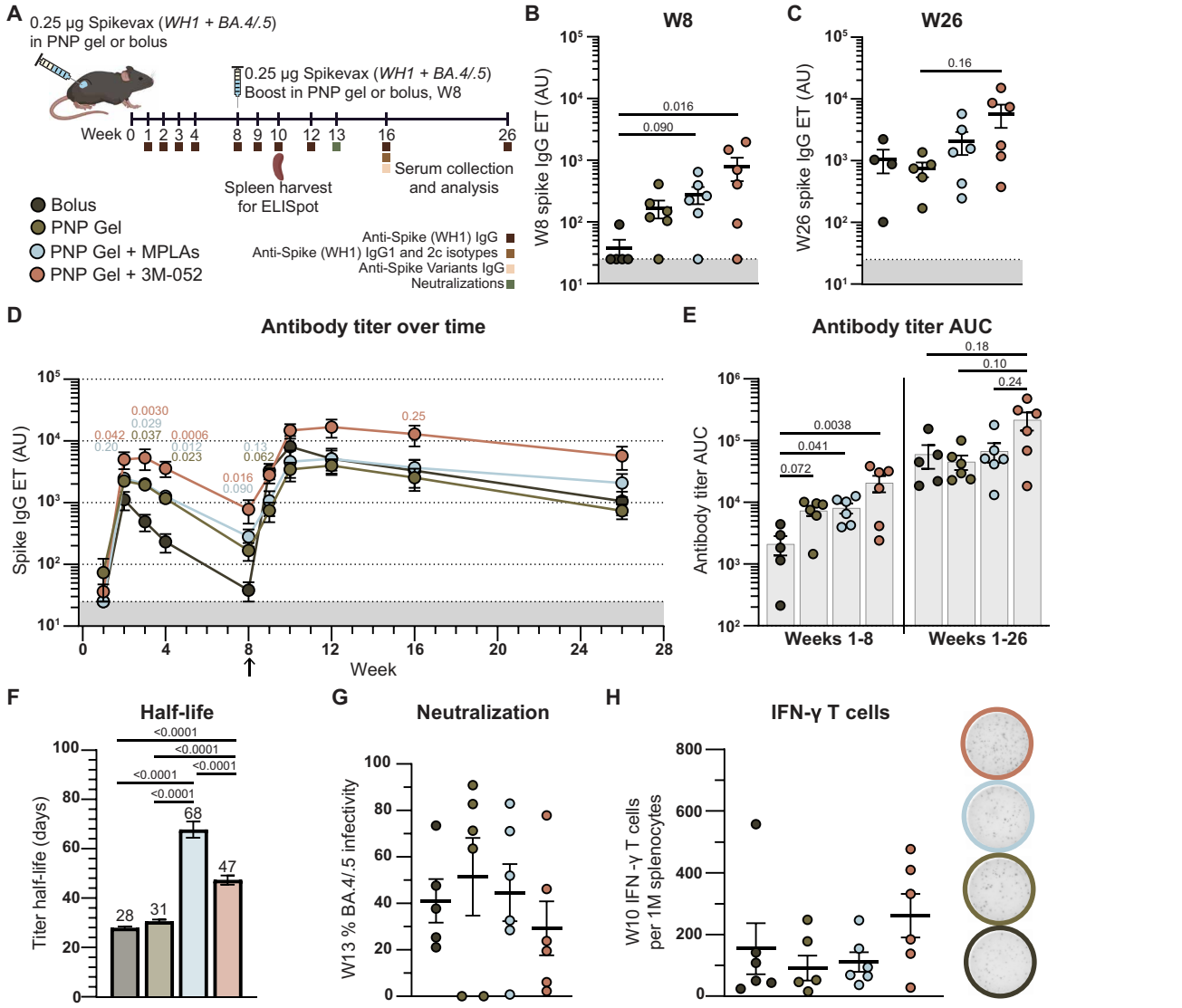

Fig. 4. Humoral response to hydrogel-based mRNA/LNP vaccines. (**A**) Mice were immunized with 0.25 µg of commercially available bivalent SARS-CoV-2 mRNA vaccine (0.125 µg of each variant) in PBS bolus or PNP-0.5-5 hydrogel with or without 1 µg of 3M-052 or 20 µg of MPLAs at week 0 and boosted with a homologous boost at week 8. Serum collected at designated time points was analyzed for anti-spike (Wuhan-Hu-1) antibodies via ELISA, as well as for other viral variant anti-spike antibodies, IgG subtypes, and neutralizing capacity. A separate cohort of animals primed and boosted in the same fashion were euthanized 2 weeks post-boost and spleens harvested for ELISpot evaluation of spike specific (WH1) T cells. Anti-WH1 spike IgG end point titers for all animals at (**B**) week 8, (**C**) week 26, and (**D**) over time. (**E**) AUC of antibody titer from week 1 to 8 (pre-boost) and 1 to 26 (full time course) per animal. (**F**) Decay half-life of antibody titer post-boost derived from parametric bootstrapping of titers following each treatment group's post-boost peak. Data shown as means ± SEM, $n = 1000$ simulations. (**G**) Percent infectivity of BA.4/.5 pseudotyped lentivirus at week 13 post-prime and 1:50 serum dilution. (**H**) Spike-specific (WH1) IFN-γ–producing splenocytes, as a proxy for T cells, at week 2 post-boost. Data shown as means ± SEM, $n = 4$ to 6. Statistical values shown are P values <0.25 obtained from GLM fitting and Tukey post hoc multiple comparison test in JMP. In (D), comparisons shown are to bolus control for the groups of the text color.

Increased breadth of humoral response to mRNA vaccine with PNP hydrogel delivery

Another important aspect of a vaccine response, particularly against highly mutable viruses like SARS-CoV-2, is the breadth of humoral responses. We evaluated antibody isotypes and end point titers at week 16 post-prime against seven SARS-CoV-2 variants of concern, as well as SARS-CoV-1 (Fig. 5, A and B). All groups exhibited similar immunoglobulin G1 (IgG1) titers, with PNP hydrogel groups showing modestly higher IgG1 titers on average compared to bolus, but only PNP hydrogels with 3M-052 produced measurable IgG2c titers in a majority of animals (four of six). The average IgG2c titer for animals immunized with PNP hydrogel and 3M-052 was significantly higher than with PNP hydrogel only and moderately higher than with bolus control ($P = 0.0055$ and 0.30, respectively). This was further reflected in the IgG2c/IgG1 ratio, a proxy for T_H1 and T_H2 skewing (Fig. 5C). While PNP hydrogels produced comparable T_H2 skewing to the bolus control, incorporation of adjuvant 3M-052 elicited a clear skewing toward T_H1. Since protection against different infectious diseases can be better mediated by different $T_H1/2$ skewing depending on the disease, the ability to tailor the response

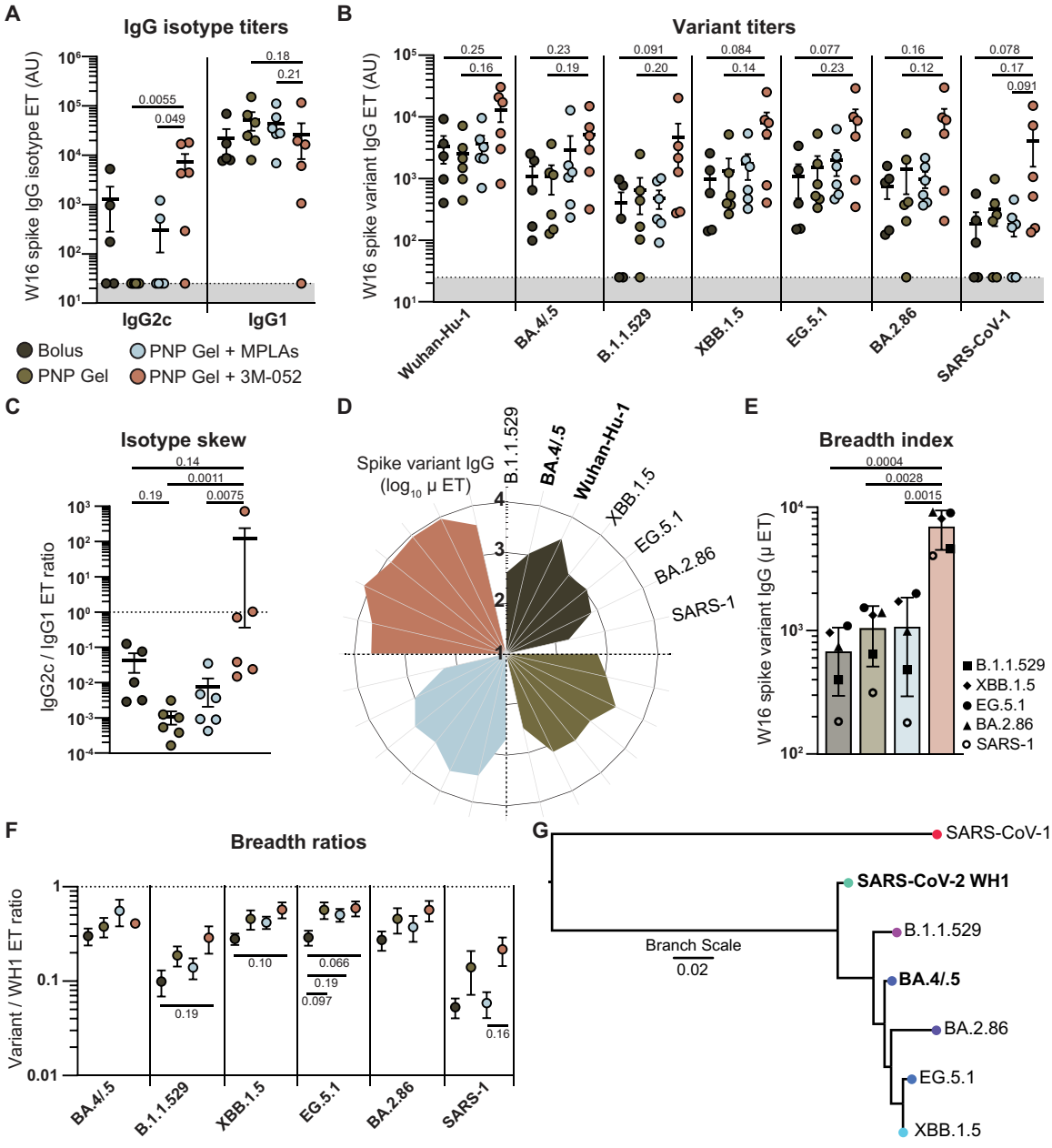

Fig. 5. Breadth and functionality of response to hydrogel-based mRNA/LNP vaccines. (**A**) IgG isotype end point titers at week 16 post-prime. (**B**) Anti-spike end point ELISA titers against different variants at week 16 post-prime. (**C**) Ratio of IgG2c to IgG1 antibody isotypes indicating T_H1 (higher values) or T_H2 (lower values) skewing. (**D**) Radar plot of absolute IgG end point titer for each variant. Broader and larger petals indicate improved breadth and consistency of response. (**E**) Quantification of (D), where each data point is the average of $n = 5$ to 6 animals against a single spike variant. Data shown as means ± SD. (**F**) Ratio of end point IgG titer for each variant compared with WH1 as a metric of consistency and breadth of humoral response. (**G**) Phylogenetic tree showing lineage of variants assessed created using "Gene/Protein Tree" tool on the Bacterial and Viral Bioinformatics Resource Center (BV-BRC) website https://bv-brc.org/. Unless otherwise written, data shown as means ± SEM, $n = 5$ to 6. Statistical values shown are P values <0.25 obtained from GLM fitting and Tukey post hoc multiple comparison test in JMP.

in a simple and modular way by just changing the admixed adjuvant coencapsulated within the PNP hydrogel is a substantial benefit (*30*).

In addition, PNP hydrogel delivery of mRNA/LNP vaccines improved the breadth of antibody titers, particularly in adjuvanted PNP hydrogel groups. A petal/radar plot of anti-spike titers across variants is one way to quickly visualize increased breadth (Fig. 5D). The PNP hydrogel group exhibited a slightly larger and broader petal than the bolus control, indicating an overall increase in antibodies against the tested variants not included in the vaccine, as well as a more consistent response across those variants. PNP hydrogel with 3M-052 elicited an even larger, broader petal than PNP hydrogel alone or with MPLAs. Of note, PNP hydrogels also reduced the number of nonresponders to some variants, like B.1.1.529 and SARS-CoV-1, over standard bolus vaccination, and PNP hydrogels

with 3M-052 produced measurable anti–SARS-CoV-1 titers in all six animals (Fig. 5B), albeit the higher absolute titers of PNP with 3M-052 animals were not statistically significant for any particular variant. We further quantified the breadth of the humoral response with an absolute breadth index composed of the average titer for animals in each treatment group against each individual variant those animals were not vaccinated against (Fig. 5E). This breadth index is slightly increased for PNP hydrogels alone and with MPLAs compared to bolus and significantly higher for PNP hydrogels with 3M-052 ($P = 0.0004$). We also evaluated the quality of breadth using a relative ratio comparing each animal's antibody titer for each variant to the titer against wild-type WH1 (Fig. 5F). This breadth ratio analysis revealed that PNP hydrogel groups elicited more consistent responses, with ratios closer to one for all variants, indicating not just higher absolute titers but anti-variant titers closer to those against wild-type WH1 despite not being represented in the vaccine. This trend, however, was not statistically significant. The variants tested span US Centers for Disease Control and Prevention variants of concern and are genetically distinct within the Omicron clade (Fig. 5G).

mRNA vaccination with PNP hydrogels improved magnitude and durability of germinal center response

To better understand the origin of the observed improvements in durability, breadth, and T cell responses imparted by PNP hydrogel delivery of mRNA/LNP vaccines with and without adjuvants, we used flow cytometry to probe the germinal center responses in draining LNs at weeks 1, 2, and 4 following prime vaccination with 0.25 μg of Moderna Spikevax bivalent vaccine (WH1 and BA.4/.5) (Fig. 6A and figs. S15 and S16). Within the first week, we observed that PNP hydrogel immunization elicited a higher proportion of activated B cells ($MHCII^+$ $CD86^+$), which was further increased with adjuvants and significantly so with 3M-052 ($P = 0.0003$) (Fig. 6B). We also found a higher light zone to dark zone (LZ:DZ) ratio after 1 week for PNP hydrogel alone ($P = 0.090$) and significantly so when adjuvanted with 3M-052 ($P = 0.0003$) compared to bolus vaccination (Fig. 6C). These improvements observed only a week after prime injection in PNP hydrogel groups were interesting considering that the slow release of cargo would lead us to expect slower germinal center kinetics compared to bolus. We hypothesize that these early increases in LN and germinal center reactions result from the unique advantage of the in vivo immune niche formed within the PNP hydrogel depots and an early boost in the response from APCs transfected in the PNP niche.

We more specifically examined the germinal center reaction by quantifying germinal center B (B_{GC}) cells, including WH1 spike–specific B_{GC} cells, and T follicular helper (T_{FH}) cells (Fig. 6, D to F). PNP hydrogels showed comparable or increased percentages of B_{GC} cells to bolus controls at all time points, with 0.29 to 0.69% in bolus and 0.56 to 0.94% in PNP hydrogel animals (Fig. 6G and fig. S17). Adjuvanting with MPLAs provided a substantive increase over bolus or PNP hydrogels alone, with B_{GC} cells comprising up to 1.19% of B cells ($P = 0.14/0.050$ at weeks 2/4 compared to bolus). PNP hydrogel adjuvanted with 3M-052 exhibited further significant improvements, up to 1.79% of B cells, compared to bolus ($P = 0.0066/0.027$ at weeks 2/4), as well as a substantive benefit over unadjuvanted PNP hydrogel ($P = 0.083/0.087$, weeks 2/4). We integrated B_{GC} cell percentages over time and observed that PNP hydrogels increased the total B_{GC} cell exposure (AUC) by 36%, and PNP hydrogel groups adjuvanted with MPLAs and 3M-052 further increased this to 44 and 149% compared to bolus ($P = 0.19$ for 3M-052). We delved further into the B_{GC} cells and quantified those that were specific for one of the mRNA encoded antigens, WH1 SARS-CoV-2 spike protein. Spike-specific B_{GC} cells were indeed found increased in PNP hydrogel groups, especially for hydrogels adjuvanted with 3M-052 as early as week 1 ($P = 0.062$ to bolus) and persisted out to 4 weeks (Fig. 6H). PNP hydrogels with MPLAs led to more spike-specific B_{GC} cells at the later time point (week 4) compared to bolus ($P = 0.18$), while the improvements for PNP hydrogels with 3M-052 were observed primarily in earlier weeks.

Examining T_{FH} cells, we observed an earlier response than B_{GC} cells, with higher percentages of T_{FH} cells evident at week 1 for PNP hydrogel–treated animals (Fig. 6I and fig. S18). T_{FH} cells comprised about 1% of $CD4^+$ helper T cells for the PNP hydrogel group, but only 0.7 to 0.87% for the bolus group and upward of 1 to 1.22% and 0.94 to 1.37% for the PNP hydrogel groups adjuvanted with MPLAs and 3M-052. PNP hydrogels with 3M-052 maintained significantly higher percentages of T_{FH} cells than bolus at weeks 1 and 2 ($P = 0.0073$ and 0.0032). PNP hydrogels with MPLAs also produced a substantively higher percentage of T_{FH} cells at week 2 than bolus ($P = 0.063$), and this enhancement continued to increase through week 4 up to 1.37%, following a similar kinetic trend seen in the spike-specific B_{GC} cell counts across vaccine groups. Integration over time corroborated that PNP hydrogels increased T_{FH} cell percentage and overall exposure, and this was further increased for PNP hydrogels with adjuvants (fig. S18C).

The ratio of B_{GC} cells to T_{FH} cells can be used as a metric for the quality of T_{FH} cell help, which we evaluated at weeks 2 and 4 (we excluded week 1 because of the weak early B_{GC} response) (Fig. 6J) (*54*). More animals exhibited consistently higher quality T_{FH} cell help in the PNP hydrogel group at week 2, with 4 in 10 animals at or above the third quartile compared with only 2 in 10 animals in the bolus group, which also had a lower third quartile value. Adjuvanting of the PNP hydrogels with MPLAs or 3M-052 further improved the quality of T_{FH} cell help, both in magnitude (average ratio) as well as number of animals experiencing better help (i.e., the spread of animals above the average), although group averages were not statistically different at week two. Week 4 ratios showed a slight waning, but adjuvanted PNP hydrogel immunization prolonged significantly better T_{FH} cell help compared to bolus ($P = 0.10/0.019$ for MPLAs/3M-052) and PNP hydrogel alone ($P = 0.21/0.046$, MPLAs/3M-052). It was clear that PNP hydrogels, particularly PNP hydrogels adjuvanted with 3M-052, improved the magnitude, duration, and quality of the germinal center reaction to mRNA/LNP vaccines, which reflected improvements in antibody titers, breadth, and durability found earlier.

DISCUSSION

In this work, we showed that delivering a commercially available SARS-CoV-2 mRNA/LNP vaccine within an injectable PNP hydrogel depot led to improved humoral and cellular immune responses driven by increased and prolonged germinal center reactions. PNP hydrogels enable facile formulation of off-the-shelf mRNA/LNPs with various adjuvant cargos, create tunable immunological niches in vivo based on different adjuvant cargos, and promote transfection of APCs within the niche without any modifications to the LNPs. We characterized incorporation of mRNA/LNPs into PNP hydrogel materials and showed that formulation in this way does not affect

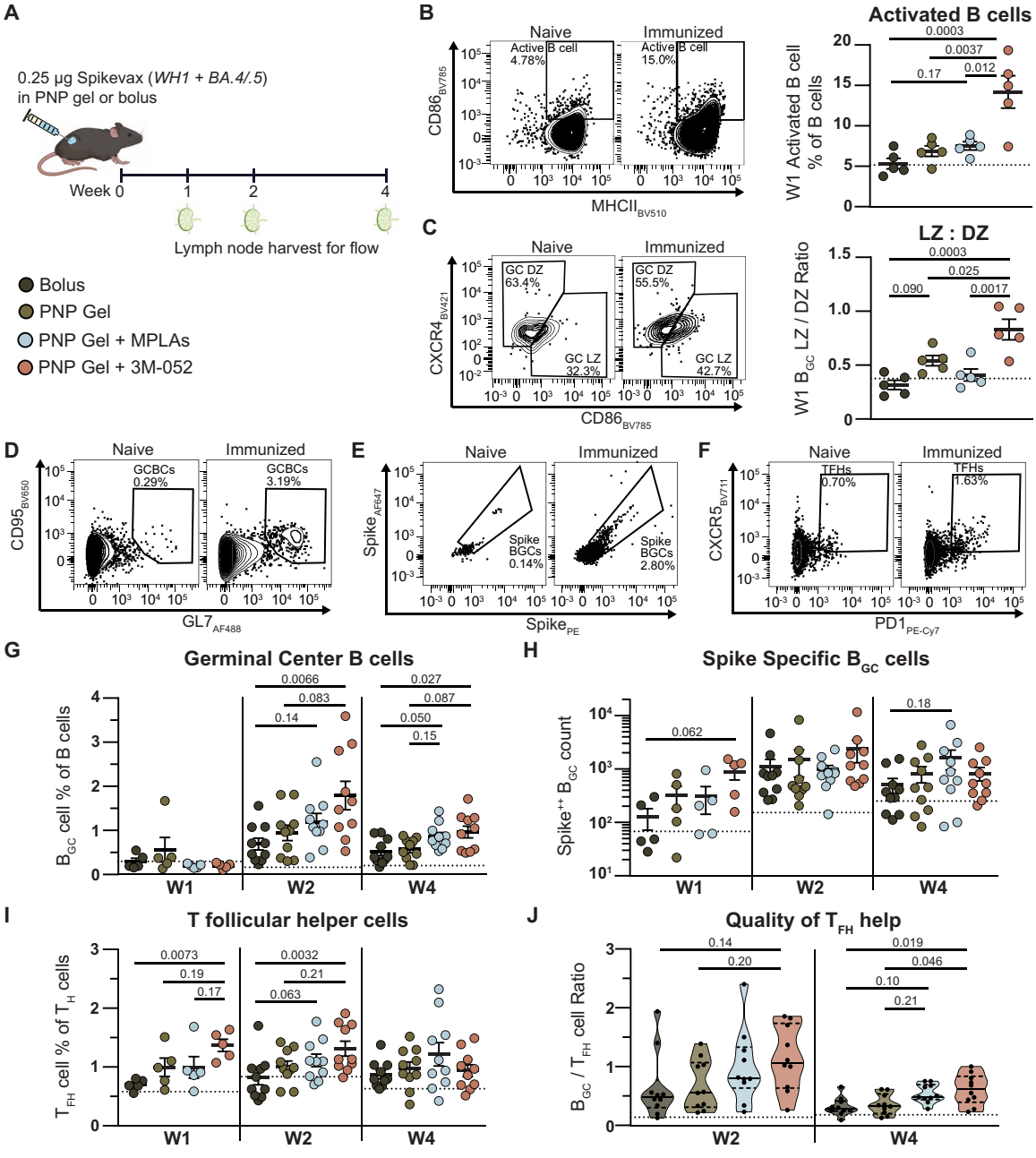

Fig. 6. Germinal center response to hydrogel-based mRNA/LNP vaccines. (**A**) Mice were immunized with bivalent SARS-CoV-2 mRNA vaccine in PBS bolus or PNP-0.5-5 hydrogel with or without adjuvants and LNs harvested at weeks 1, 2, and 4. Week 1 representative flow plots and quantification of (**B**) activated B cells ($B220^+$ $MHCII^+$ $CD86^+$) and (**C**) light and dark zone B_{GC} cells ($B220^+$ $CD95^-$ $GL7^+$ $CD38^-$ $CD86^+$ $CXCR4^-$ and $CD86^-$ $CXCR4^+$). (**D**) Representative flow plots of B_{GC} cells ($B220^+$ $CD95^-$ $GL7^+$), (**E**) spike-specific B_{GC} cells ($CD38^-$ $Spike^{++}$), and (**F**) T_{FH} ($CD19^-$ $CD3^+$ $CD4^+$ $CXCR5^+$ $PD\text{-}1^+$). Percentages of parent population except $Spike^{++}$ B_{GC} cells, which are of grandparent (see supplemental gating strategy). (**G**) Quantification of B_{GC} cell percentage of all B cells. (**H**) Counts of $Spike^{++}$ B_{GC} cells. (**I**) Quantification of T_{FH} cell percentage of all $CD4^+$ T cells. (**J**) Ratio of B_{GC} cells to T_{FH} cells as a metric of T_{FH} cell help quality. All data shown as means ± SEM, $n = 5$ to 10. Statistical values shown are P values <0.25, obtained from GLM fitting and Tukey post hoc multiple comparison test in JMP.

material properties or LNP transfection efficiency. We then characterized the cellular milieu within the PNP hydrogel depot in vivo and determined it to be highly plastic and tunable based on incorporation of adjuvant cargo. We further showed that key APCs within this niche preferentially expressed delivered mRNA. Following this characterization, we showed that immunization with commercial mRNA/LNP vaccine in a PNP hydrogel niche with and without adjuvants improved the efficacy of Moderna Spikevax over clinically relevant bolus controls. In particular, PNP hydrogels enhanced mRNA/LNP vaccines in key areas for improvement of current mRNA/LNP vaccines, including durability and breadth of the humoral response, and were otherwise equivalent or noninferior in

areas considered sufficient with current mRNA/LNP vaccines, like neutralization. Last, we investigated the germinal center reactions driving observed improvements in humoral and cellular responses and found that PNP hydrogel delivery of mRNA/LNP vaccine increased the magnitude, duration, and quality of LN germinal center reactions. This work represented an exploratory investigation of mRNA/LNP vaccination using PNP materials with and without adjuvants and, hence, was powered to detect large observations. However, follow-up studies should be conducted to confirm significance of key trends presented here, such as the improved antibody titers against different spike protein variants for animals vaccinated with PNP hydrogel and 3M-052.

In contrast to chemical strategies to target LNPs to APCs, our approach does not require altering LNPs and can be readily applied to commercially available mRNA/LNP vaccines. Furthermore, these PNP hydrogels may be more widely applicable to other mRNA and nucleic acid delivery platforms like poly(β-amino esters) or viral vectors, although this would require further study (*3*). We found the best humoral response and most active germinal center reactions in animals immunized with PNP hydrogels adjuvanted with 3M-052, a potent TLR7/8 agonist, yet this hydrogel niche was found to host the fewest DCs and instead comprised substantially more transfected monocytes than other tested groups (Figs. 3 and 4). We initially hypothesized that better vaccine responses would positively correlate with the presence of DCs in the PNP hydrogel niche; however, these data indicate that this is not necessarily the case and highlight an important gap in knowledge in the field. There are few studies characterizing cellular recruitment to vaccine injection sites or understanding correlations between injection site cellular milieu and strong or specific mounted immune responses. This shortfall is due in part to fundamental difficulties in measuring cells within an injection site, particularly in the subcutaneous space. While some research has attempted to characterize the immune infiltrate following intramuscular or intradermal vaccine injections, many studies have relied heavily on imaging modalities and immunohistochemistry approaches requiring biopsies of an injection site that can be difficult to find reproducibly (*8*, *55*). One of the key advantages of the PNP platform is that it allows us to study vaccine injection site reactions with single-cell resolution in a way previously not possible. Future work could consider additional processing, like single-cell sequencing and cytokine profiling, to further elucidate differences at the injection site, which may correlate to overall shifts in the downstream immune responses.

This work contributes to an exciting and growing field exploring how biomaterials can interface with the body and immune system through cellular niche formation (*15*–*22*). It remains an open question how the cellular niche in PNP hydrogels is spatially distributed. While there were relatively few B and T cells in the hydrogel compared to innate cells, it would be interesting to characterize whether these cells are in close spatial proximity or possibly forming a tertiary lymphoid structure with active B and T cell training. Future work could explore this with immunohistochemistry and co-detection by indexing techniques.

In addition to the immune niche benefit of the PNP hydrogel, the material further allows simple mixing of unmodified adjuvants. While adjuvants are known to improve the immune response to protein antigens, adjuvanting mRNA vaccines is complicated and undercharacterized, requiring a balanced approach as excessive immune activation and cytokine production can hamper mRNA translation (*56*). Adjuvants, particularly TLR agonists, exhibit a wide range of physiochemical properties, from small molecules to large single- or double-stranded nucleic acid chains, which make their interactions with mRNA vaccines difficult to study in a systematic or modular fashion. It is important to more thoroughly understand the impact of adjuvants on mRNA vaccines, as well as to find adjuvants that improve and tailor vaccine responses for different antigens or diseases. Prior works adjuvanting mRNA vaccines have focused on incorporating adjuvants into LNPs, often requiring modifications to both the adjuvant and the particle formulation and are generally nontransferable to other adjuvant molecules. The PNP hydrogel platform provides a unique means to independently incorporate adjuvants alongside mRNA/LNPs, allowing for unprecedented control over adjuvanting mRNA vaccines and investigating the impact on immune responses. In this work, we found that TLR4 activation by MPLAs has little benefit over PNP hydrogel delivery alone, but TLR7/8 activation by 3M-052 significantly improved the magnitude and quality of vaccine responses. Other depot technologies such as alum are known to produce a strong T_H2-skewed response even when combined with T_H1-skewing adjuvants like 3M-052, yet the PNP hydrogels alone are rather inert and do not modulate T_H skewing (Fig. 5), giving more modular and independent control of T_H skewing through incorporated adjuvants (*57*).

Future work could explore other adjuvants targeting different TLRs, such as TLR1/2a (Pam3CSK4), TLR9a (CpG), or STING (cGAMP), as well as combinations of adjuvants shown in other contexts to afford synergistic immune activation (*30*, *58*, *59*). In addition, the PNP hydrogel platform enables encapsulation of other immune activating cargo in a plug-and-play manner, like protein chemokines or cytokines, that would otherwise be difficult or impossible to codeliver with mRNA/LNPs without modification (*41*). Granulocyte-macrophage colony-stimulating factor is a small protein that should drive infiltration of more DCs into the PNP material and could be combined with other adjuvants. Cytokines like interleukin-10 (IL-10) or IL-2 could also be incorporated to induce a more tolerogenic niche in the PNP hydrogel (*60*, *61*). The modularity of this platform can effectively skew the immunological niche and subsequent response based on encapsulated molecular cargos, creating opportunities beyond improving infectious disease vaccines to directing improved cytotoxic responses in cancer vaccines or suppressive responses in tolerogenic applications.

While PNP delivery of mRNA/LNPs offers a lot of potential to improve vaccine efficacy as well as introduce a platform to study the impact of adjuvants and the injection site kinetics in a way otherwise unstudied, there remains work to be done. One limitation of the presented work is that it focuses on a single target disease, SARS-CoV-2, and does not expand to other antigens that may show different responses. In addition, the PNP hydrogel niche is characterized at two time points, but mRNA expression is transient and some immune cells have very short lifespans (e.g., only 3 days for neutrophils) (*62*). Follow-up work should evaluate the kinetics of the immune niche and mRNA expression in greater depth and at additional time points, as well as investigate the kinetics of antigen and cellular accumulation in the LNs. Furthermore, this work could be conducted in Ai14/Cre mice to allow analysis of all cells which translate delivered mRNA, not just the ones currently expressing enough protein to be detected (*63*). This would further allow decoupling of cellular expression of encoded protein from the possibility

that cells within the PNP niche are phagocytosing protein made by other transfected cells in the niche. Together, the presented work shows that PNP hydrogel delivery of mRNA/LNPs is a promising strategy to use a tunable immunomodulatory platform for a variety of applications, ranging from probing fundamental questions about injection site cellular reactions to mRNA vaccines, to improving vaccine efficacy against infectious diseases without altering LNP chemistries, and even potential to tailor proinflammatory or tolerogenic responses.

MATERIALS AND METHODS

PNP hydrogel formulation

HPMC-C_{12} and PEG-PLA were prepared as described in Supplemental Methods. HPMC-C_{12} was dissolved at 2 wt % in PBS and loaded into a 1-ml Luer-Lock syringe. A 20–wt % solution of PEG-PLA NPs in PBS was added to a solution of PBS with or without mRNA/LNPs and/or adjuvant depending on formulation and loaded into a second 1-ml syringe. The two syringes were connected with a female-female Luer-Lock elbow, with care to avoid air at the interface of the HPMC-C_{12} and nanoparticle solution, and gently mixed until a homogenous PNP hydrogel was formed. Hydrogels were formulated with final concentrations of 0.5 or 1 wt % HPMC-C_{12} and 5 wt % NPs, denoted PNP-0.5-5 or PNP-1-5.

PNP hydrogel rheological characterization

Rheological characterization was performed on PNP hydrogels with or without Moderna Spikevax monovalent (50 μg ml^{-1}) using a TA Instruments DHR-2 stress-controlled rheometer. All experiments were performed using a 20-mm-diameter serrated plate geometry at 25°C with a 500-μm gap. Frequency sweep measurements were performed at a constant 1% strain in the linear viscoelastic regime. Stress sweeps were performed from low to high with steady-state sensing and yield stress values defined as the stress at the intersection of lines tangent to the plateau and the yielding regimes. Flow sweeps were performed from high to low shear rates. Step shear experiments were performed by alternating between a low shear rate (0.1 s^{-1}; 60 s) and a high shear rate (10 s^{-1}; 30 s) for three cycles.

In vitro LNP transfection

RAW-Blue cells (InvivoGen, raw-sp) were cultured at 37°C with 5% CO_2 in Dulbecco's modified Eagle's medium (DMEM) supplemented with high glucose, L-glutamine, sodium pyruvate (Cytiva, SH30243.FS), 10% heat-inactivated fetal bovine serum (FBS, Cytiva, SH30396.03HI), and penicillin (100 U ml^{-1})–streptomycin (100 μg ml^{-1}) (Cytiva, SV30010). Cells (100 k) were plated in each well of a tissue culture–treated 96-well plate in 200 μl of medium and allowed to adhere for 24 hours. After 24 hours, the medium was aspirated, replaced with 180 μl of fresh medium, and 20 μl of PNP hydrogel or PBS with luciferase mRNA/LNPs (5 μg ml^{-1}) (collaborators in the Irvine group at MIT) was injected through a 26-gauge needle into each well (n = 3 to 4 wells) for a final concentration of 0.1 μg per well. The plate was incubated for 24 hours and transfection efficiency measured using Bright-Glo Luciferase Assay System (Promega). Briefly, 100 μl of BrightGlo reagent was added to each well, and, after a 3-min incubation, 180 μl from each well was transferred to a white 96-well plate and luminescence was read on a Synergy H1 Microplate Reader (BioTek Instruments).

Mice and vaccination

All animal studies were performed in accordance with the National Institutes of Health guidelines, with the approval of the Stanford Administrative Panel on Laboratory Animal Care (protocol APLAC-32109). Seven- to eight-week-old female C57BL/6 were purchased from Charles River and housed in the animal facility at Stanford University. The mice were shaved and injected through a 26-gauge needle subcutaneously on the right flank with 100 μl of either bolus or gel vaccine under brief isoflurane anesthesia. Unless noted otherwise, the mice were injected within 5 weeks of arriving at Stanford. Blood was collected weekly from tail veins. For flow cytometry, the mice were euthanized under CO_2, and organs such as inguinal LN and spleen were explanted or hydrogels were explanted from the subcutaneous space.

Vaccine and other formulations

Vaccine primes and boosts (8 weeks after prime) contained 0.25 μg of Moderna Spikevax bivalent (WH1 and BA.4/.5, 0.125 μg of each variant) per dose in either bolus (PBS) or in PNP hydrogels with or without 20 μg per dose MPLAs (InvivoGen, vac-mpls) or 1 μg per dose 3M-052 [material transfer agreement with Access to Advanced Health Institute (AAHI)]. Bolus adjuvant experiments used 0.25 μg of Moderna Spikevax monovalent (XBB.1.5) alone or with 1 μg/20 μg 3M-052/alum (AAHI) per dose in PBS. Spikevax was obtained from the Stanford Hospital Pharmacy and stored at 4°C until use within 7 days of first septa puncture, or frozen at −20°C and only thawed once before use. For gel infiltration studies, 1 μg per dose of mCherry encoding mRNA/LNPs was incorporated into PNP hydrogels and dosed. mRNA/LNPs encoding mCherry or firefly luciferase were prepared via nanoprecipitation and commercially available lipids mimicking the Moderna Spikevax formulation. Briefly, SM-102 (BroadPharm), DSPC (Avanti Polar Lipids), cholesterol (Avanti Polar Lipids), and PEG-DMG 2000 (Avanti Polar Lipids) were dissolved in ethanol in the molar ratio 50:10:38.5:1.5 to make a lipid solution. mRNA with 5-methoxyuridine modification encoding mCherry or firefly luciferase (TriLink) was dissolved in citrate butter (pH 3). LNPs were formulated by mixing lipid and mRNA solutions in the ratio 1:3 (v/v) at 12 ml min^{-1} using an Ignite NanoAssemblr (Precision Nanosystems). LNPs were dialyzed overnight against 20 mM tris acetate and 8% (w/v) RNAse-free sucrose (VWR) using 3500 MWCO dialysis cassettes (Thermo Fisher Scientific), aliquoted, and stored at −80°C until use.

Flow cytometry of PNP hydrogel immune infiltrate

The mice were shaved and injected subcutaneously on the right flank with 100 μl of PNP-0.5-5 hydrogels with mCherry mRNA/LNPs (1 μg $dose^{-1}$), with or without MPLAs or 3M-052. At 3 and 7 days after injection, the mice were euthanized by CO_2 and hydrogel depots extracted and placed in microcentrifuge tubes with 750 μl fluorescence-activated cell sorting (FACS) buffer (PBS, 3% heat-inactivated FBS, and 1 mM EDTA). Hydrogels were mechanically disrupted to single-cell suspensions using Kimble BioMasherIIs (DWK Life Sciences). Suspensions were passed through a 70-μm cell filter (Celltreat, 229484) into 15-ml Falcon tubes, spun at 500 rcf for 5 min, resuspended in PBS, and counted using acridine orange/propidium iodide cell viability stain (Vitascientific, LGBD10012) and a Luna-FL dual Fluorescence cell counter (Logos biosystems). One million live cells per sample were transferred to a 96-well conical bottom plate (Thermo Fisher Scientific, 249570) and stained.

Mouse serum ELISAs

Antigen-specific IgG end point titers were measured using an end point ELISA. MaxiSorp plates (Thermo Fisher Scientific, 449824) were coated with SARS-CoV-2 spike trimer (Sino Biological, 40589-V08H4) or variant trimer (Sino Biological, 40589-V08H32, 40589-V08H26, 40589-V08H45, 40589-V08H55, 40589-V08H58, or 40634-V08B) at 2 μg ml^{-1} in PBS at 4°C overnight and subsequently stored at −80°C. The plates were thawed for 1 to 2 hours at room temperature, washed five times with 300 μl per well wash solution (PBS with 0.05% Tween 20), and blocked with diluent buffer (PBS with 1% bovine serum albumin) for 2 hours. All incubation steps were at room temperature on a rotator, and the plates were washed five times with wash solution between each step. Serum dilutions were prepared during the blocking step in a conical bottom plate (Thermo Fisher Scientific, 249570) in diluent buffer starting at 1:100 (1 μl of serum into 99 μl of diluent buffer) and serially diluted fourfold. Following blocking and washing, serum dilutions were transferred to antigen-coated plate, 50 μl per well, and incubated for 2 hours. Goat anti-mouse IgG Fc horseradish peroxidase (HRP, Invitrogen, A16084) was diluted from glycerol stock (1 mg ml^{-1}) into diluent buffer (1:10,000) and 50 μl added to each well and incubated for 1 hour. For isotype ELISAs, goat anti-mouse IgG1 or IgG2c heavy-chain HRP (Abcam, ab97240 or ab97255) were diluted 1:20,000 from vendor stock solution. The plates were developed for 6 min with high-sensitivity tetramethylbenzidine (TMB) substrate (Abcam, ab171523), and the reaction was stopped with 1 N HCl. Absorbance was read at 450 nm with a Synergy H1 microplate reader (BioTek Instruments). Data were analyzed in GraphPad Prism and fit with a five-point asymmetric sigmoidal curve with constraints $S > 0$, top <4, and bottom = 0.048 (background absorbance value). The end point titer was defined as the serum dilution value at which the absorbance reached 2× the background value, or 0.1, interpolated from the curve fits in GraphPad Prism. For isotype plates, background absorbance was set to 0.094 and 0.066 for IgG1 and 2c, respectively, and end point was defined at 0.2. Samples below end point absorbance at 1:100 dilution were designated below the limit of detection and the end point titer defined as a dilution value of 25.

Serum neutralization assays against pseudoviruses

Antisera were heat inactivated (56°C, 30 to 60 min) before neutralization assays. Neutralization against SARS-CoV-2 BA.4/5 was analyzed in HeLA-ACE2/TMPRSS2 cells. One day before infection (day 0), cells were seeded at 8000 cells per well in white-walled, white-bottom, 96-well plates (Thermo Fisher Scientific or Greiner Bio-One). On day 1, antisera were serially diluted in D10 media and mixed 1:1 with pseudoviruses for 1 to 2 hours at 37°C before being transferred to cells. The pseudovirus mixture contained SARS-CoV-2 BA.4/5, D10 media and polybrene (1:500). The assays were read out with luciferase substrates 2 days after infection by removing the media from the wells and adding 80 μl of a 1:1 dilution of BriteLite in Dulbecco's Phosphate-Buffered Saline (BriteLite Plus, PerkinElmer). Luminescence values were measured using a microplate reader (BioTek Synergy HT or Tecan M200). Percent infection was normalized on each plate. Neutralization assays were performed in technical duplicates.

ELISpot

Spike-specific IFN-γ–producing splenocytes were evaluated using a mouse IFN-γ single color ELISpot Kit (CTL) and CTL counter (Immunospot S6 Ultra M2). Spleens were harvested from mice 2 weeks post-boost, disrupted to single-cell suspensions with frosted glass slides in CTL test media (CTLT-005) supplemented with 1% L-glutamine (termed CTL-g), passed through 70-μm cell filters into 15-ml Falcon tubes, and spun at 400 rcf for 4 min. Red blood cells were lysed with 1 ml of ACK lysis buffer (Gibco, Thermo Fisher Scientific, A1049201) for 2 min, and the reaction was quenched with 9 ml of CTL-g. Samples were spun at 400 rcf for 4 min, resuspended in CTL-g, counted, and plated in a low-bind 96-well conical bottom plate. The samples were transferred to precoated ELISpot plates and stimulated for 24 hours at 37°C with either SARS-CoV-2 pan-spike peptides (5 μg peptide^{-1} ml^{-1}; JPT Peptide Technologies, PM-WCPV-S-1), concanavalin A (ConA, 1 μg ml^{-1}; Sigma-Aldrich, C0412-5MG) as a positive control, or CTL-g as a negative control. The cells were at a final concentration of 200 k in negative wells, 400 k in ConA wells, and both 200 and 400 k in peptide wells. After 24 hours, the spots were developed following the manufacturer's instructions.

Flow cytometry of LNs

Draining inguinal LNs were harvested from mice at weeks 1, 2, and 4 post-prime. LNs were disrupted, filtered, and counted as previously described in hydrogel preparation, and 1 million live cells per sample were transferred to a 96-well conical bottom plate and stained.

Staining protocol and panels

LN and hydrogel samples were first stained with 100 μl of Live/Dead Fixable Near-IR (Thermo Fisher Scientific, L34975) for 30 min at room temperature, quenched with 100 μl of FACS buffer, and spun at 935 rcf for 2 min. The samples were then incubated with 50 μl of anti-mouse CD16/CD32 (1:50 dilution; BD, 553142) for 5 min on ice before incubating with 50 μl of full antibody stain for 40 min on ice for hydrogel samples and 60 min for LN samples. The samples were spun and resuspended in 50 to 70 μl of FACS buffer and run on the BD FACSymphony A5 SORP in the Stanford Shared FACS Facility. Data were analyzed in FlowJo and fluorescence minus one controls (FMOs) used to inform gating strategies.

LN full antibody stain included anti-CD184 (1:400 dilution; BV421; Thermo Fisher Scientific, 50-605-189), anti-CD138 (1:400; BV605; Thermo Fisher Scientific, 50-207-1399), anti-CD86 (1:400; BV785; Thermo Fisher Scientific, NC1188484), anti-CD279 [1:400; phycoerythrin (PE)–Cy7; BioLegend, 135215], anti-CD19 (1:200; PerCP/Cy5.5; Thermo Fisher Scientific, 50-113-0313), anti-CD95 (1:200; BV650; Thermo Fisher Scientific, BDB740507), anti-CD38 (1:200; BUV737; BD, 741748), anti-CD4 (1:200; BUV805; BD, 612900), anti–I-A/I-E (1:200; BV510; BioLegend, 107636), anti-GL7 (1:100; AF488; Thermo Fisher Scientific, 50-711-897), anti-CD3 (1:100; AF700; Thermo Fisher Scientific, 50-162-375), anti-CD45R (1:100; BUV395; BD, 563793), anti-CD185 (1:50; BV711; Thermo Fisher Scientific, 50-207-1644), anti-spike tetramer (20 nM; AF647), and anti-spike tetramer (20 nM; PE). Tetramers were prepared on ice by adding AF647- or PE-streptavidin (Thermo Fisher Scientific, S32357 or BD, 554061) to 6 μM biotinylated wild-type SARS-CoV-2 spike trimer (Sino Biological, 40589-V27B-B) in five steps, once every 20 to 60 min, for a final molar ratio of 4.1:1 spike protein to dye and concentration of 0.5 μM.

Hydrogel full antibody stain included the following: anti–I-A/I-E (1:800 dilution; fluorescein isothiocyanate; BioLegend, 107605), anti-CD45 (1:800; AF700; BioLegend, 103127), anti-Ly6C (1:400; BV570; BioLegend, 128029), anti-XCR1 (1:200; AF647; BioLegend, 148213), anti-F4/80 (1:200; BV421; BioLegend, 123137), anti-Ly6G (1:200; BV711; BioLegend, 127643), anti-CD3e (1:200; PerCP-eFluor710; Thermo Fisher Scientific, 46-0033-82), anti-CD19 (1:200; PE-Cy7;

BioLegend, 115519), anti-CD11c (1:200; PE; BioLegend, 117307), anti-CD11b (1:100; BV510; Thermo Fisher Scientific, 50-112-9846), and anti-NK1.1 (1:100; BV605; BioLegend, 108753).

Statistical analysis

For in vivo experiments, the animals were cage blocked in all experiments except the humoral study and data presented as means ± SEM. Comparisons between multiple groups were conducted with the general linear model and Tukey post hoc test in JMP, accounting for cage blocking. To normalize variance and meet requirements for statistical tests used, flow cytometry data presented as percentages (e.g., B_{GC} cells percent of B cells) were transformed using the equation $y = \ln[x/(100 - x)]$, where x is the original data point and y the data subject to statistical tests. ELISA titer data and flow cytometry cell counts presented on log plots were similarly transformed by $y = \log_{10}(x)$. Comparisons between two groups were conducted with multiple unpaired two-tailed Student's t tests run in GraphPad Prism with false discovery rate correction using two-stage step-up method of Benjamini, Krieger. Select P values are shown in the text and figures, and all P values are in the Supplementary Materials.

Supplementary Materials

The PDF file includes:
Supplementary Methods
Figs. S1 to S18
Tables S1 to S22
Legend for data file S1

Other Supplementary Material for this manuscript includes the following:
Data file S1

REFERENCES AND NOTES

1. N. Chaudhary, D. Weissman, K. A. Whitehead, mRNA vaccines for infectious diseases: Principles, delivery and clinical translation. *Nat. Rev. Drug Discov.* **20**, 817–838 (2021).
2. X. Hou, T. Zaks, R. Langer, Y. Dong, Lipid nanoparticles for mRNA delivery. *Nat. Rev. Mater.* **6**, 1078–1094 (2021).
3. K. Paunovska, D. Loughrey, J. E. Dahlman, Drug delivery systems for RNA therapeutics. *Nat. Rev. Genet.* **23**, 265–280 (2022).
4. M. Echaide, L. Chocarro de Erauso, A. Bocanegra, E. Blanco, G. Kochan, D. Escors, mRNA vaccines against SARS-CoV-2: Advantages and caveats. *Int. J. Mol. Sci.* **24**, 5944 (2023).
5. N. Pardi, M. J. Hogan, D. Weissman, Recent advances in mRNA vaccine technology. *Curr. Opin. Immunol.* **65**, 14–20 (2020).
6. Z. Sun, T. Wu, H. Xie, Y. Li, J. Zhang, X. Su, H. Qi, The role of cellular immunity in the protective efficacy of the SARS-CoV-2 vaccines. *Vaccine* **10**, 1103 (2022).
7. P. Midoux, C. Pichon, Lipid-based mRNA vaccine delivery systems. *Expert Rev. Vaccines* **14**, 221–234 (2015).
8. K. J. Hassett, I. L. Rajlic, K. Bahl, R. White, K. Cowens, E. Jacquinet, K. E. Burke, mRNA vaccine trafficking and resulting protein expression after intramuscular administration. *Mol. Ther. Nucleic Acids* **35**, 102083 (2024).
9. X. Zhuang, Y. Qi, M. Wang, N. Yu, F. Nan, H. Zhang, M. Tian, C. Li, H. Lu, N. Jin, mRNA vaccines encoding the HA protein of influenza A H1N1 virus delivered by cationic lipid nanoparticles induce protective immune responses in mice. *Vaccine* **8**, 123 (2020).
10. D. Tarab-Ravski, L. Stotsky-Oterin, D. Peer, Delivery strategies of RNA therapeutics to leukocytes. *J. Control. Release* **342**, 362–371 (2022).
11. R. Kedmi, N. Veiga, S. Ramishetti, M. Goldsmith, D. Rosenblum, N. Dammes, I. Hazan-Halevy, L. Nahary, S. Leviatan-Ben-Arye, M. Harlev, M. Behlke, I. Benhar, J. Lieberman, D. Peer, A modular platform for targeted RNAi therapeutics. *Nat. Nanotechnol.* **13**, 214–219 (2018).
12. L. M. Kranz, M. Diken, H. Haas, S. Kreiter, C. Loquai, K. C. Reuter, M. Meng, D. Fritz, F. Vascotto, H. Hefesha, C. Grunwitz, M. Vormehr, Y. Hüsemann, A. Selmi, A. N. Kuhn, J. Buck, E. Derhovanessian, R. Rae, S. Attig, J. Diekmann, R. A. Jabulowsky, S. Heesch, J. Hassel, P. Langguth, S. Grabbe, C. Huber, Ö. Türeci, U. Sahin, Systemic RNA delivery to dendritic cells exploits antiviral defence for cancer immunotherapy. *Nature* **534**, 396–401 (2016).
13. C. Hald Albertsen, J. A. Kulkarni, D. Witzigmann, M. Lind, K. Petersson, J. B. Simonsen, The role of lipid components in lipid nanoparticles for vaccines and gene therapy. *Adv. Drug Deliv. Rev.* **188**, 114416 (2022).
14. K. Kobiyama, K. J. Ishii, Making innate sense of mRNA vaccine adjuvanticity. *Nat. Immunol.* **23**, 474–476 (2022).
15. J. D. Griffin, J. Y. Song, A. Huang, A. R. Sedlacek, K. L. Flannagan, C. J. Berkland, Antigen-specific immune decoys intercept and exhaust autoimmunity to prevent disease. *Biomaterials* **222**, 119440 (2019).
16. S. M. Azarin, J. Yi, R. M. Gower, B. A. Aguado, M. E. Sullivan, A. G. Goodman, E. J. Jiang, S. S. Rao, Y. Ren, S. L. Tucker, V. Backman, J. S. Jeruss, L. D. Shea, In vivo capture and label-free detection of early metastatic cells. *Nat. Commun.* **6**, 8094 (2015).
17. D. K. Y. Zhang, J. M. Brockman, K. Adu-Berchie, Y. Liu, Y. Binenbaum, I. de Lázaro, M. C. Sobral, R. Tresa, D. J. Mooney, Subcutaneous biodegradable scaffolds for restimulating the antitumour activity of pre-administered CAR-T cells. *Nat. Biomed. Eng.* **9**, 268–278 (2025).
18. S. Pacelli, S. Basu, J. Whitlow, A. Chakravarti, F. Acosta, A. Varshney, S. Modaresi, C. Berkland, A. Paul, Strategies to develop endogenous stem cell-recruiting bioactive materials for tissue repair and regeneration. *Adv. Drug Deliv. Rev.* **120**, 50–70 (2017).
19. R. M. Raghani, R. R. Urie, J. A. Ma, G. Escalona, I. A. Schrack, K. M. DiLillo, P. Kandagatla, J. T. Decker, A. H. Morris, K. B. Arnold, J. S. Jeruss, L. D. Shea, Engineered immunologic niche monitors checkpoint blockade response and probes mechanisms of resistance. *ImmunoMedicine* **4**, e1052 (2024).
20. Y. M. Yoon, J. S. Lewis, M. R. Carstens, M. Campbell-Thompson, C. H. Wasserfall, M. A. Atkinson, B. G. Keselowsky, A combination hydrogel microparticle-based vaccine prevents type 1 diabetes in non-obese diabetic mice. *Sci. Rep.* **5**, 13155 (2015).
21. R. Allen, S. Chizari, J. A. Ma, S. Raychaudhuri, J. S. Lewis, Combinatorial, microparticle-based delivery of immune modulators reprograms the dendritic cell phenotype and promotes remission of collagen-induced arthritis in mice. *ACS Appl. Bio. Mater.* **2**, 2388–2404 (2019).
22. K. Adu-Berchie, J. M. Brockman, Y. Liu, T. W. To, D. K. Y. Zhang, A. J. Najibi, Y. Binenbaum, A. Stafford, N. Dimitrakakis, M. C. Sobral, M. O. Dellacherie, D. J. Mooney, Adoptive T cell transfer and host antigen-presenting cell recruitment with cryogel scaffolds promotes long-term protection against solid tumors. *Nat. Commun.* **14**, 3546 (2023).
23. Y. Mochida, S. Uchida, mRNA vaccine designs for optimal adjuvanticity and delivery. *RNA Biol.* **21**, 1–27 (2024).
24. C. Xie, R. Yao, X. Xia, The advances of adjuvants in mRNA vaccines. *NPJ Vaccines* **8**, 162 (2023).
25. S. Linares-Fernández, C. Lacroix, J.-Y. Exposito, B. Verrier, Tailoring mRNA vaccine to balance innate/adaptive immune response. *Trends Mol. Med.* **26**, 311–323 (2020).
26. O. A. W. Haabeth, J. J. K. Lohmeyer, A. Sallets, T. R. Blake, I. Sagiv-Barfi, D. K. Czerwinski, B. McCarthy, A. E. Powell, P. A. Wender, R. M. Waymouth, R. Levy, An mRNA SARS-CoV-2 vaccine employing charge-altering releasable transporters with a TLR-9 agonist induces neutralizing antibodies and T cell memory. *ACS Cent. Sci.* **7**, 1191–1204 (2021).
27. Y. Gu, J. Yang, C. He, T. Zhao, R. Lu, J. Liu, X. Mo, F. Wen, H. Shi, Incorporation of a Toll-like receptor 2/6 agonist potentiates mRNA vaccines against cancer and infectious diseases. *Signal Transduct. Target. Ther.* **8**, 273 (2023).
28. X. Han, M.-G. Alameh, K. Butowska, J. J. Knox, K. Lundgreen, M. Ghattas, N. Gong, L. Xue, Y. Xu, M. Lavertu, P. Bates, J. Xu, G. Nie, Y. Zhong, D. Weissman, M. J. Mitchell, Adjuvant lipidoid-substituted lipid nanoparticles augment the immunogenicity of SARS-CoV-2 mRNA vaccines. *Nat. Nanotechnol.* **18**, 1105–1114 (2023).
29. B. Li, A. Y. Jiang, I. Raji, C. Atyeo, T. M. Raimondo, A. G. R. Gordon, L. H. Rhym, T. Samad, C. MacIsaac, J. Witten, H. Mughal, T. M. Chicz, Y. Xu, R. P. McNamara, S. Bhatia, G. Alter, R. Langer, D. G. Anderson, Enhancing the immunogenicity of lipid-nanoparticle mRNA vaccines by adjuvanting the ionizable lipid and the mRNA. *Nat. Biomed. Eng.* **9**, 167–184 (2025).
30. A. Kaur, J. Baldwin, D. Brar, D. B. Salunke, N. Petrovsky, Toll-like receptor (TLR) agonists as a driving force behind next-generation vaccine adjuvants and cancer therapeutics. *Curr. Opin. Chem. Biol.* **70**, 102172 (2022).
31. H. H. Tam, M. B. Melo, M. Kang, J. M. Pelet, V. M. Ruda, M. H. Foley, J. K. Hu, S. Kumari, J. Crampton, A. D. Baldeon, R. W. Sanders, J. P. Moore, S. Crotty, R. Langer, D. G. Anderson, A. K. Chakraborty, D. J. Irvine, Sustained antigen availability during germinal center initiation enhances antibody responses to vaccination. *Proc. Natl. Acad. Sci. U.S.A.* **113**, E6639–E6648 (2016).
32. D. J. Irvine, A. Aung, M. Silva, Controlling timing and location in vaccines. *Adv. Drug Deliv. Rev.* **158**, 91–115 (2020).
33. J. H. Lee, H. J. Sutton, C. A. Cottrell, I. Phung, G. Ozorowski, L. M. Sewall, R. Nedellec, C. Nakao, M. Silva, S. T. Richey, J. L. Torres, W.-H. Lee, E. Georgeson, M. Kubitz, S. Hodges, T.-M. Mullen, Y. Adachi, K. M. Cirelli, A. Kaur, C. Allers, M. Fahlberg, B. F. Grasperge, J. P. Dufour, F. Schiro, P. P. Aye, O. Kalyuzhniy, A. Liguori, D. G. Carnathan, G. Silvestri, X. Shen, D. C. Montefiori, R. S. Veazey, A. B. Ward, L. Hangartner, D. R. Burton, D. J. Irvine, W. R. Schief, S. Crotty, Long-primed germinal centres with enduring affinity maturation and clonal migration. *Nature* **609**, 998–1004 (2022).

34. K. Bloom, F. van den Berg, P. Arbuthnot, Self-amplifying RNA vaccines for infectious diseases. *Gene Ther.* **28**, 117–129 (2021).
35. E. A. Appel, M. W. Tibbitt, M. J. Webber, B. A. Mattix, O. Veiseh, R. Langer, Self-assembled hydrogels utilizing polymer–nanoparticle interactions. *Nat. Commun.* **6**, 6295 (2015).
36. G. A. Roth, E. C. Gale, M. Alcántara-Hernández, W. Luo, E. Axpe, R. Verma, Q. Yin, A. C. Yu, H. Lopez Hernandez, C. L. Maikawa, A. A. A. Smith, M. M. Davis, B. Pulendran, J. Idoyaga, E. A. Appel, Injectable hydrogels for sustained codelivery of subunit vaccines enhance humoral immunity. *ACS Cent. Sci.* **6**, 1800–1812 (2020).
37. E. C. Gale, A. E. Powell, G. A. Roth, E. L. Meany, J. Yan, B. S. Ou, A. K. Grosskopf, J. Adamska, V. C. T. M. Picece, A. I. d'Aquino, B. Pulendran, P. S. Kim, E. A. Appel, Hydrogel-based slow release of a receptor-binding domain subunit vaccine elicits neutralizing antibody responses against SARS-CoV-2. *Adv. Mater.* **33**, e2104362 (2021).
38. J. Yan, B. S. Ou, O. M. Saouaf, E. L. Meany, N. Eckman, E. A. Appel, A regimen compression strategy for commercial vaccines leveraging an injectable hydrogel depot technology for sustained vaccine exposure. *Adv. Therap.* **7**, 2300108 (2024).
39. O. M. Saouaf, G. A. Roth, B. S. Ou, A. A. A. Smith, A. C. Yu, E. C. Gale, A. K. Grosskopf, V. C. T. M. Picece, E. A. Appel, Modulation of injectable hydrogel properties for slow co-delivery of influenza subunit vaccine components enhance the potency of humoral immunity. *J. Biomed. Mater. Res. A* **109**, 2173–2186 (2021).
40. S. Correa, E. L. Meany, E. C. Gale, J. H. Klich, O. M. Saouaf, A. T. Mayer, Z. Xiao, C. S. Liong, R. A. Brown, C. L. Maikawa, A. K. Grosskopf, J. L. Mann, J. Idoyaga, E. A. Appel, Injectable nanoparticle-based hydrogels enable the safe and effective deployment of immunostimulatory CD40 agonist antibodies. *Adv. Sci.* **9**, 2103677 (2022).
41. A. K. Grosskopf, L. Labanieh, D. D. Klysz, G. A. Roth, P. Xu, O. Adebowale, E. C. Gale, C. K. Jons, J. H. Klich, J. Yan, C. L. Maikawa, S. Correa, B. S. Ou, A. I. d'Aquino, J. R. Cochran, O. Chaudhuri, C. L. Mackall, E. A. Appel, Delivery of CAR-T cells in a transient injectable stimulatory hydrogel niche improves treatment of solid tumors. *Sci. Adv.* **8**, eabn8264 (2022).
42. E. L. Meany, R. Andaya, S. Tang, C. M. Kasse, R. N. Fuji, A. K. Grosskopf, A. L. d'Aquino, J. T. Bartoe, R. Ybarra, A. Shelton, Z. Pederson, C. Hu, D. Leung, K. Nagapudi, S. Ubhayakar, M. Wright, C.-W. Yen, E. A. Appel, Injectable polymer-nanoparticle hydrogel for the sustained intravitreal delivery of bimatoprost. *Adv. Therap.* **6**, 2200207 (2023).
43. B. S. Ou, O. M. Saouaf, J. Yan, T. U. J. Bruun, J. Baillet, X. Zhou, N. P. King, E. A. Appel, Broad and durable humoral responses following single hydrogel immunization of SARS-CoV-2 subunit vaccine. *Adv. Healthc. Mater.* **12**, e2301495 (2023).
44. C. M. Kasse, A. C. Yu, A. E. Powell, G. A. Roth, C. S. Liong, C. K. Jons, A. Buahin, C. L. Maikawa, X. Zhou, S. Youssef, J. E. Glanville, E. A. Appel, Subcutaneous delivery of an antibody against SARS-CoV-2 from a supramolecular hydrogel depot. *Biomater. Sci.* **11**, 2065–2079 (2023).
45. A. I. d'Aquino, C. L. Maikawa, L. T. Nguyen, K. Lu, I. A. Hall, C. K. Jons, C. M. Kasse, J. Yan, A. N. Prossnitz, E. Chang, S. W. Baker, L. Hovgaard, D. B. Steensgaard, H. B. Andersen, L. Simonsen, E. A. Appel, Use of a biomimetic hydrogel depot technology for sustained delivery of GLP-1 receptor agonists reduces burden of diabetes management. *Cell Rep. Med.* **4**, 101292 (2023).
46. S. P. Kasturi, M. A. U. Rasheed, C. Havenar-Daughton, M. Pham, T. Legere, Z. J. Sher, Y. Kovalenkov, S. Gumber, J. Y. Huang, R. Gottardo, W. Fulp, A. Sato, S. Sawant, S. Stanfield-Oakley, N. Yates, C. LaBranche, S. M. Alam, G. Tomaras, G. Ferrari, D. Montefiori, J. Wrammert, F. Villinger, M. Tomai, J. Vasilakos, C. B. Fox, S. G. Reed, B. F. Haynes, S. Crotty, R. Ahmed, B. Pulendran, 3M-052, a synthetic TLR-7/8 agonist, induces durable HIV-1 envelope–specific plasma cells and humoral immunity in nonhuman primates. *Sci. Immunol.* **5**, eabb1025 (2020).
47. K. O. Saunders, E. Lee, R. Parks, D. R. Martinez, D. Li, H. Chen, R. J. Edwards, S. Gobeil, M. Barr, K. Mansouri, S. M. Alam, L. L. Sutherland, F. Cai, A. M. Sanzone, M. Berry, K. Manne, K. W. Bock, M. Minai, B. M. Nagata, A. B. Kapingidza, M. Azoitei, L. V. Tse, T. D. Scobey, R. L. Spreng, R. W. Rountree, C. T. DeMarco, T. N. Denny, C. W. Woods, E. W. Petzold, J. Tang, T. H. Oguin, G. D. Sempowski, M. Gagne, D. C. Douek, M. A. Tomai, C. B. Fox, R. Seder, K. Wiehe, D. Weissman, N. Pardi, H. Golding, S. Khurana, P. Acharya, H. Andersen, M. G. Lewis, I. N. Moore, D. C. Montefiori, R. S. Baric, B. F. Haynes, Neutralizing antibody vaccine for pandemic and pre-emergent coronaviruses. *Nature* **594**, 553–559 (2021).
48. J. Wang, X.-G. Yin, Y. Wen, J. Lu, R.-Y. Zhang, S.-H. Zhou, C.-M. Liao, H.-W. Wei, J. Guo, MPLA-adjuvanted liposomes encapsulating S-trimer or RBD or S1, but not S-ECD, elicit robust neutralization against SARS-CoV-2 and variants of concern. *J. Med. Chem.* **65**, 3563–3574 (2022).
49. C. K. Jons, A. K. Grosskopf, J. Baillet, J. Yan, J. H. Klich, O. M. Saouaf, E. A. Appel, Yield-stress and creep control depot formation and persistence of injectable hydrogels following subcutaneous administration. *Adv. Funct. Mater.* **32**, 2203402 (2022).
50. G. A. Roth, V. C. T. M. Picece, B. S. Ou, W. Luo, B. Pulendran, E. A. Appel, Designing spatial and temporal control of vaccine responses. *Nat. Rev. Mater.* **7**, 174–195 (2022).
51. Z. Zhang, D. Procissi, W. Li, D.-H. Kim, K. Li, G. Han, Y. Huan, A. C. Larson, High resolution MRI for non-invasive mouse lymph node mapping. *J. Immunol. Methods* **400-401**, 23–29 (2013).
52. R. Mead, *The Design of Experiments: Statistical Principles for Practical Applications*. (Cambridge Univ. Press, 1990).
53. F. Faul, E. Erdfelder, A. G. Lang, A. Buchner, G*Power 3: A flexible statistical power analysis program for the social, behavioral, and biomedical sciences. *Behav. Res. Methods* **39**, 175–191 (2007).
54. C. Havenar-Daughton, D. G. Carnathan, A. Torrents de la Peña, M. Pauthner, B. Briney, S. M. Reiss, J. S. Wood, K. Kaushik, M. J. van Gils, S. L. Rosales, P. van der Woude, M. Locci, K. M. Le, S. W. de Taeye, D. Sok, A. U. R. Mohammed, J. Huang, S. Gumber, A. Garcia, S. P. Kasturi, B. Pulendran, J. P. Moore, R. Ahmed, G. Seumois, D. R. Burton, R. W. Sanders, G. Silvestri, S. Crotty, Direct probing of germinal center responses reveals immunological features and bottlenecks for neutralizing antibody responses to HIV Env trimer. *Cell Rep.* **17**, 2195–2209 (2016).
55. F. Liang, G. Lindgren, A. Lin, E. A. Thompson, S. Ols, J. Röhss, S. John, K. Hassett, O. Yuzhakov, K. Bahl, L. A. Brito, H. Salter, G. Ciaramella, K. Loré, Efficient targeting and activation of antigen-presenting cells in vivo after modified mRNA vaccine administration in rhesus macaques. *Mol. Ther.* **25**, 2635–2647 (2017).
56. M. P. Lokugamage, Z. Gan, C. Zurla, J. Levin, F. Z. Islam, S. Kalathoor, M. Sato, C. D. Sago, P. J. Santangelo, J. E. Dahlman, Mild innate immune activation overrides efficient nanoparticle-mediated RNA delivery. *Adv. Mater.* **32**, e1904905 (2020).
57. D. Li, D. R. Martinez, A. Schäfer, H. Chen, M. Barr, L. L. Sutherland, E. Lee, R. Parks, D. Mielke, W. Edwards, A. Newman, K. W. Bock, M. Minai, B. M. Nagata, M. Gagne, D. C. Douek, C. T. DeMarco, T. N. Denny, T. H. Oguin, A. Brown, W. Rountree, Y. Wang, K. Mansouri, R. J. Edwards, G. Ferrari, G. D. Sempowski, A. Eaton, J. Tang, D. W. Cain, S. Santra, N. Pardi, D. Weissman, M. A. Tomai, C. B. Fox, I. N. Moore, H. Andersen, M. G. Lewis, H. Golding, R. Seder, S. Khurana, R. S. Baric, D. C. Montefiori, K. O. Saunders, B. F. Haynes, Breadth of SARS-CoV-2 neutralization and protection induced by a nanoparticle vaccine. *Nat. Commun.* **13**, 6309 (2022).
58. K. K. Short, S. M. Miller, L. Walsh, V. Cybulski, H. Bazin, J. T. Evans, D. Burkhart, Co-encapsulation of synthetic lipidated TLR4 and TLR7/8 agonists in the liposomal bilayer results in a rapid, synergistic enhancement of vaccine-mediated humoral immunity. *J. Control. Release* **315**, 186–196 (2019).
59. R. Toy, M. C. Keenum, P. Pradhan, K. Phang, P. Chen, C. Chukwu, L. A. H. Nguyen, J. Liu, S. Jain, G. Kozlowski, J. Hosten, M. S. Suthar, K. Roy, TLR7 and RIG-I dual-adjuvant loaded nanoparticles drive broadened and synergistic responses in dendritic cells in vitro and generate unique cellular immune responses in influenza vaccination. *J. Control. Release* **330**, 866–877 (2021).
60. T. Mohan, W. Zhu, Y. Wang, B.-Z. Wang, Applications of chemokines as adjuvants for vaccine immunotherapy. *Immunobiology* **223**, 477–485 (2018).
61. C. D. Moorman, S. J. Sohn, H. Phee, Emerging therapeutics for immune tolerance: Tolerogenic vaccines, T cell therapy, and IL-2 therapy. *Front. Immunol.* **12**, 657768 (2021).
62. D. Polak, B. Bohle, Neutrophils-typical atypical antigen presenting cells? *Immunol. Lett.* **247**, 52–58 (2022).
63. K. J. Kauffman, M. A. Oberli, J. R. Dorkin, J. E. Hurtado, J. C. Kaczmarek, S. Bhadani, J. Wyckoff, R. Langer, A. Jaklenec, D. G. Anderson, Rapid, single-cell analysis and discovery of vectored mRNA transfection in vivo with a loxP-flanked tdTomato reporter mouse. *Mol. Ther. Nucleic Acids* **10**, 55–63 (2018).

Acknowledgments: We would like to thank every member of the Appel Lab, former and current, for their on-going support, technical expertise, and scientific discussion. In particular, we thank S. Reyes, C. (Lyla) Dong, A. Singh, P. Ganesh, I. Ajifolokun, J. Yan, and L. T. Nguyen for assistance with tissue dissociation. We also thank V. Böhnert for help in designing an initial flow cytometry panel for PNP hydrogel cell infiltration. **Funding:** This research was financially supported in part by the Bill & Melinda Gates Foundation (OPP1113682, OPP1211043, INV027411, and INV-010680). E.L.M. was supported by the NIH Biotechnology Training Program (T32-GM008412). B.S.O. was supported by Eastman Kodak Fellowship. C.K.J., O.M.S., S.C.W., and N.E. were supported by the National Science Foundation Graduate Research Fellowship. O.M.S. was also supported by the Hancock Fellowship of the Stanford Graduate Fellowship in Science and Engineering. T.M. was supported by the Jane Coffin Childs Postdoctoral Fellowship. A.U. was supported by the Stanford University Medical Scientist Training Program (T32-GM007365 and T32-GM145402). Flow cytometry data were collected on an instrument in the Stanford Shared FACS Facility obtained using NIH S10 Shared Instrument Grant (1S10OD026831-01). **Author contributions:** Conceptualization: E.L.M., D.J.I., and E.A. Methodology: E.L.M., A.U., O.M.S., and E.A. Software: E.L.M. and N.E. Validation: E.L.M. Formal analysis: E.L.M., C.K.J., and A.U. Investigation: E.L.M., J.H.K., C.K.J., N.C., A.U., J.B., Y.E.S., O.M.S., B.S.O., and S.C.W. Resources: T.M., N.C., D.J.I., and E.A. Data curation: E.A. Writing—original draft: E.L.M. and N.C. Writing—review and editing: E.L.M., J.H.K., T.M., A.U., J.B., S.C.W., D.J.I., and E.A. Visualization: E.L.M. Supervision: D.J.I. and E.A. Project administration: D.J.I. and E.A. Funding acquisition: D.J.I. and E.A. **Competing interests:** E.L.M., E.A., and B.S.O. are inventors on provisional patent applications related to this work. The authors declare that they have no other competing interests. **Data and materials availability:** All data needed to evaluate the conclusions in the paper are present in the paper and/or the Supplementary Materials. All materials are

commercially available, and methods for their synthesis are provided in Materials and Methods. Source data for flow cytometry data and analysis in Figs. 2, 3, and 6 and the supplementary figures can be found on the Dryad database online at DOI: 10.5061/dryad.8931zcs1t.

Submitted 24 June 2024
Accepted 7 March 2025
Published 11 April 2025
10.1126/sciadv.adr2631